Carpathian Journal of Earth and Environmental Sciences, August 2020, Vol. 15, No. 2, p. 491 – 514; Doi:10.26471/cjees/2020/015/148

MULTI-STAGE REORGANIZATIONS OF FELDSPARS IN FELSIC ROCKS OF THE DITRĂU ALKALINE INTRUSIVE COMPLEX, ROMANIA

Gabriel BINDEA[1], Satoshi NAKANO[2] & Kuniaki MAKINO[3]

[1]*Geological Institute of Romania, Caransebes nr. 1, Bucharest, Ro 012271, Romania, bindeagabi@yahoo.com*
[2]*Faculty of Education, Shiga University, Hiratsu 5-2-1, Otsu 520-0862, Japan (Present address: Lake Biwa Museum, Oroshimo 1090, Kusatsu 525-0001, Japan)*
[3]*Faculty of Science, Shinshu University, Asahi 3-1-1, Matsumoto 390-8621, Japan*

Abstract: This paper describes notable characteristics of feldspars in felsic rocks of the Ditrău alkaline intrusive complex, Eastern Carpathians, Romania. Microtextures and compositions of feldspars in samples of monzonite, syenite, nepheline syenite and granite belonging to four geological units of the Ditrău complex have been examined. Plagioclase grains mostly of albite compositions show intricate boundaries with microperthitic alkali feldspar grains. It is the most striking texture in alkali feldspars that large albite cores or remnants are often enclosed by low microcline with saw-tooth or lamellar boundaries, which coexist with various microperthitic textures. Microperthites consisting of low microcline (K-feldspar) with tartan twinning and low albite show diverse textural heterogeneities in the size (width), shape and distribution of constituent albite associated with cryptoperthitic~fine-microperthitic lamellae. In contrast, it is also remarkable that clear K-feldspar areas heterogenously coexist with microperthitic~meso-microperthitic areas in individual alkali feldspars. Most of the compositions of constituent albite and microcline are close to the end-members through the rocks. They are estimated to have been produced by multi-stage reactions from the higher-temperature magmatic to lower-temperature reorganization through the exsolution stage. The latest albitization and K-feldspathization ultimately overprinted or reorganized magmatic resorption and subsolidus exsolution textures and compositions.

Keywords: albite, microcline, microperthite, albitization, K-feldspathization, replacement, felsic rock, Ditrău

1. INTRODUCTION

The Ditrău alkaline intrusive complex (DAIC) is a famous, classical of geology and petrology. Since its discovery by Herbich (1872), many workers have studied the DAIC consisting of a large variety of rock types with complicated field relationships (Streckeisen, 1931~1960; Codarcea et al., 1957; Streckeisen & Hunziker, 1974; Anastasiu & Constantinescu, 1982; Dallmeyer et al., 1997; Morogan et al., 2000; Pană et al., 2000; Bonin et al., 2002; Pál-Molnár et al., 2015a, b). From detailed field surveys, Kräutner & Bindea (1998) proposed a three-stage igneous activity of the DAIC with geochronological data existing at the time (Streckeisen & Hunziker, 1974; Dallmeyer et al., 1997) from ca. 230 Ma of mafic and ultramafic rocks, through ca. 215 Ma of gabbros, diorites, granites, monzonites, and syenites, to 165-160 Ma of nepheline syenites, which imply long and repeated episodes of fluid-rock reaction. They also pointed out hydrothermal activity with abundant volatiles throughout the complex. Thereafter, Morogan et al., (2000) proposed that a variety of rock types might have been derived at the early stage of magmatic evolution with a significant role of volatiles. The alkaline character and abundant volatiles are also proved by the presence of mantle-derived lamprophyre dykes such as camptonite (Batki et al., 2014). However, affecting roles of such abundant volatiles on the resultant characters of the DAIC rocks have not been so studied to date.

Concerning this problem, mineralogical studies of the DAIC rocks using modern methods have been rarely made, although Batki et al., (2018) elucidated the crystallization evolution of the pyroxenes. Such studies focusing feldspars in the DAIC felsic rocks are lack at present, in spite of the

recently accumulated, fruitful knowledge of feldspar mineralogy (e.g., Deer et al., 2001). In this context, this study has focused on the DAIC feldspars. We have found that there are common features of feldspar textures and compositions, especially in their microperthitic textures, through the different geological units and host rocks. The obtained data show that the feldspars in the examined DAIC felsic rocks underwent multi-stage reorganizations, especially low-temperature reactions mediated by abundant volatiles. This paper outlines such notable characters of the feldspars through the examined samples.

2. GEOLOGICAL OUTLINE

The following brief geological outline of the DAIC is extracted from Kräutner & Bindea (1998) and Morogan et al., (2000). The DAIC is exposed in the hinterland of the Eastern Carpathians fold-and-thrust belt, in the southern part of the "Crystalline-Mesozoic Zone", near the Neogene volcanic arc. It is a Mesozoic composite intrusive complex consisting of six sub-complexes (geological units), which was incorporated in the Alpine Bucovinian Nappe during the Mid-Cretaceous shortening. The Bucovinian thrust fault cuts the DAIC at a depth of about 1800m. The DAIC pierces all the pre-Alpine (Variscan) nappes that outcrop near the intrusive contact (Kräutner & Bindea, 1998). The Alpine evolution of the Carpathian orocline, started with Triassic rifting and oceanic crust generation along the Tethys domain and continued with the Cretaceous-Tertiary subduction and collision of crustal fragments during the convergence between Europe and Africa.

Mesozoic igneous activity associated with different tectonic events took place in different pre-Alpine metamorphic terranes of the Carpathian area. The DAIC is an example of A-type igneous activity in Alpine Europe (Fig. 1). The geometry and the spatial distribution of petrographically distinct rock types in the DAIC suggest a dome shape with an imperfect ring structure (Streckeisen, 1954). An ideal model, in space, is that the DAIC is like a mafic core enveloped by various petrographical covers, which became more alkaline or more acidic toward the rim.

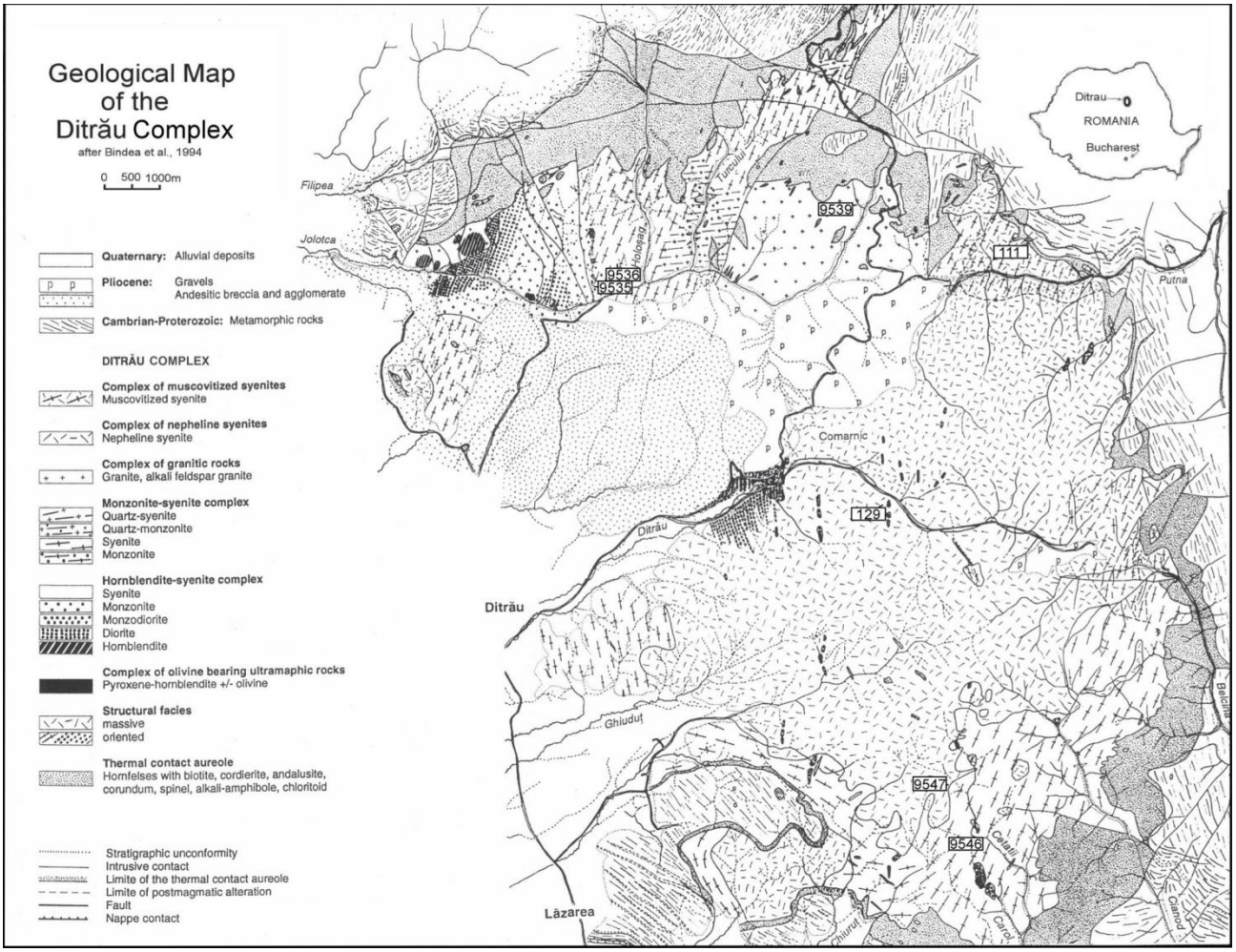

Figure 1. Sampling localities plotted on the geological map of the Ditrău complex (after Bindea G., Runceanu M., Robu I., Robu L. (1994) Unpubl. report. Arch. Geol. Inst. of Romania)

It is cut by several major faults. The most important one trends E-W and separates two regions: Jolotca area in the north dominated by saturated igneous products, consisting of ultramafics, gabbro~diorite, monzonite, alkali granite and syenite, and the southern area characterized by the presence of mostly undersaturated igneous products, from "ditro-essexite" (term introduced by Streckeisen, 1954) to nepheline syenite. Thus, the asymmetry from the northern part seems to have been produced by the uplift of the mafic complexes. The fault is exposed only in the western part of the DAIC, the rest being covered by Neogene andesitic breccia belonging to the volcanic arc and Pliocene or alluvial deposits (Fig. 1).

3. ROCK SAMPLES

The selected 7 samples are from the four felsic units in the DAIC (Table 1). The sampling localities are shown in Figure 1. Sample 111 (syenite) is from the Complex of muscovitized syenites. Samples 129 and 9547 (nepheline syenites) are from the Complex of nepheline syenites. Sample 9539 (granite) is from the Complex of granites. The rest three samples are from the Monzonite-syenite complex; the sample 9546 is a monzonite with a foliation, and the samples 9536 and 9535 are syenites. Samples 9547, 9546 and 9536 are sporadically associated with larger alkali feldspar (Af) grains, or somewhat porphyritic. Thin section microphotographs of the rocks are shown in Fig. 2A. Back-scattered electron (BSE) maps show petrographic textures of the samples at larger scale (Fig. 2B), although grain boundaries of feldspars with different orientations are not recognized in them. It is clear in the maps that alkali feldspar (Af) and plagioclase (Pl) grains are tangled with each other, and both feldspars irregularly interpenetrate each other or contact with intricate boundaries throughout the samples (Fig. 2B).

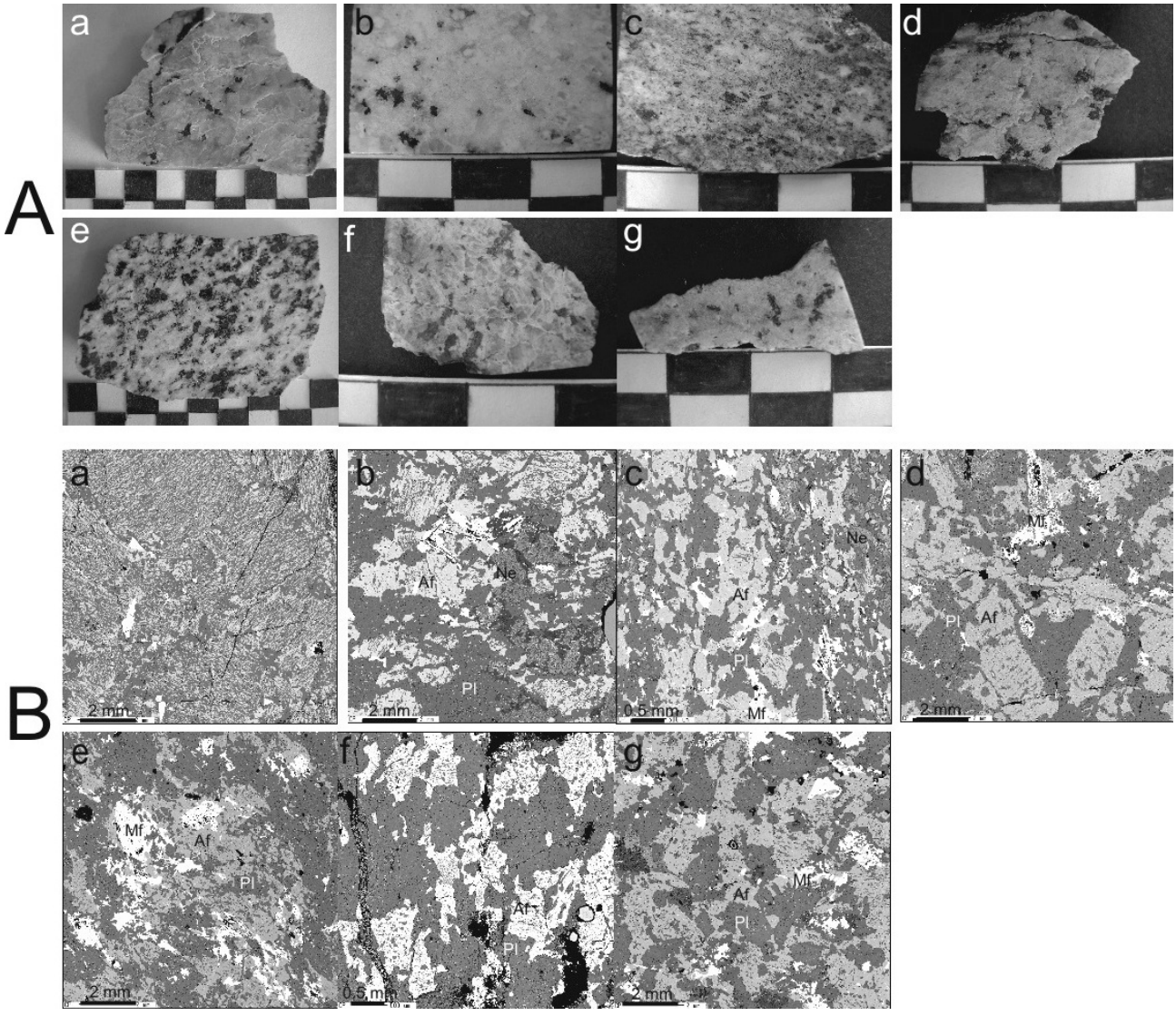

Figure 2. Close-up photographs of thin-section making chips and large scale BSE (back-scattered electron) maps showing petrographic textures of the seven Ditrău felsic rocks. (a) the sample 111, (b) 129, (c) 9547, (d) 9539, (e) 9546, (f) 9536 and (f) 95435. Mf = mafic mineral.

Table 1. Examined rock samples, their feldspar compositions and mineral assemblages.

Sample No.	**111**	**129**	**9547**	**9539**
Location	Putna Valley	Ditrău Valley	Cetății Valley	Creanga Valley
Rock unit	Complex of mucovitized syenites	Complex of nepheline syenites	Complex of nepheline syenites	Complex of granitic rocks
Rock type	syenite	nepheline syenite	nepheline syenite	Granite
Af aver. composition	$Or_{41}Ab_{59}An_{0.4}$ (121)	$Or_{48}Ab_{52}An_{0.}$ $(53)_1$	$Or_{76}Ab_{24}An_{0.6}$ (135)*	$Or_{82}Ab_{18}An_{0.6}$ (63)
Pl composition	$Ab_{96.7}An_{0.5}Or_{2.8}$~$Ab_{99.4}An_{0.3}Or_{0.2}$	$Ab_{98.7}An_{0.1}Or_{1.1}$~$Ab_{99.4}An_{0.1}Or_{0.3}$	$Ab_{93.8}An_{3.4}Or_{2.8}$~$Ab_{99.0}An_{0.5}Or_{0.4}$	$Ab_{92.0}An_{6.6}Or_{1.4}$~$Ab_{98.5}An_{1.3}Or_{0.2}$
MP** Or-rich phase Or-Ab-An/-Cn (aver.)	$Or_{96.8}Ab_{3.1}An_{0.1}$ / $Or_{96.7}Ab_{3.1}An_{0.1}Cn_{0.1}$ (32)	$Or_{94.9}Ab_{5.1}An_{0.0}$ / $Or_{94.4}Ab_{5.0}An_{0.0}Cn_{0.5}$ (43)	$Or_{96.1}Ab_{3.8}An_{0.1}$ / $Or_{94.8}Ab_{3.7}An_{0.1}Cn_{1.4}$ (32)*	$Or_{96.6}Ab_{3.3}An_{0.1}$ / $Or_{96.0}Ab_{3.3}An_{0.1}Cn_{0.6}$ (19)
BaO (range in wt%)	0.00~0.28 (aver.=0.04)	0.00~0.25 (aver.=0.15)	0.25~0.76 (aver.=0.41)	0.07~0.35 (aver.=0.17)
FeO (range in wt%)	0.00~0.21	0.00~0.08	0.00~0.10	0.01~0.14
MP Ab-rich phase Ab-An-Or/-Cn (aver.)	$Ab_{98.5}An_{1.1}Or_{0.4}$ / $Ab_{98.5}An_{1.1}Or_{0.4}Cn_{0.1}$ (38)	$Ab_{99.0}An_{0.5}Or_{0.5}$ ~ $Ab_{98.9}An_{3.8}Or_{0.6}Cn_{0.1}$ (37)	$Ab_{95.6}An_{3.8}Or_{0.6}$ / $Ab_{95.5}An_{3.8}Or_{0.6}Cn_{0.1}$ (48)*	$Ab_{92.2}An_{7.1}Or_{0.8}$ / $Ab_{92.18}An_{7.0}Or_{0.8}Cn_{0.1}$ (19)
BaO (range in wt%)	0.00~0.11 (aver.=0.02)	0.00~0.17 (aver.=0.03)	0.00~0.15 (aver.=0.02)	0.00~0.13 (aver.=0.02)
FeO (range in wt%)	0.02~0.21	0.00~0.10	0.00~0.17	0.00~0.16
Assemblage of other Ms***	Bt, Rt, Cal, Chl	Bt	Bt, Amp, Ttn, Hem, Ilm, Chl	Chl, Rt, Cal

Sample No.	**9546**	**9536**	**9535**
Location	Cetății Valley	Holoșag Valley	Simo Valley
Rock unit	Monzonite-syenite complex	Monzonite-syenite complex	Monzonite-syenite complex
Rock type	monzonite	syenite	monzonite
Af aver. composition	$Or_{74}Ab_{25}An_{1.5}$ (90)	$Or_{80}Ab_{18}An_{1.1}$ (58)	$Or_{77}Ab_{22}An_{0.1}$ (50)
Pl composition	$Ab_{85.9}An_{13.64}Or_{0.4}$~$Ab_{98.5}An_{1.1}Or_{0.5}$	$Ab_{83.5}An_{15.7}Or_{0.9}$~$Ab_{96.8}An_{2.9}Or_{0.3}$	$Ab_{85.9}An_{13.7}Or_{0.48}$~$Ab_{98.9}An_{0.6}Or_{0.4}$
MP Or-rich phase Or-Ab-An/-Cn (aver.)	$Or_{95.6}Ab_{4.3}An_{0.1}$ / $Or_{93.8}Ab_{4.2}An_{0.1}Cn_{1.9}$ (22)	$Or_{95.4}Ab_{4.48}An_{0.1}$ / $O_{91.4}Ab_{4.2}An_{0.1}Cn_{4.3}$ (28)	$Or_{96.3}Ab_{3.6}An_{0.0}$ / $Or_{95.4}Ab_{3.6}An_{0.0}Cn_{1.0}$ (30)
BaO (range in wt%)	0.28~0.83 (aver.=0.56)	0.76~1.94 (aver.=1.24)	0.05~0.77 (aver.=0.28)
FeO (range in wt%)	0.00~0.09	0.00~0.08	0.00~0.06
MP Ab-rich phase Ab-An-Or/-Cn (aver.)	$Ab_{87.3}An_{12.2}Or_{0.6}$ / $Ab_{87.2}An_{12.2}Or_{0.7}Cn_{0.1}$ (41)	$Ab_{85.9}An_{13.4}Or_{0.7}$ / $Ab_{85.8}An_{13.4}Or_{0.7}Cn_{0.2}$ (63)	$Ab_{89.5}An_{9.9}Or_{0.;7}$ / $Ab_{89.4}An_{9.9}Or_{0.7}Cn_{0.1}$ (70)
BaO (range in wt%)	0.00~0.09 (aver.=0.03)	0.00~0.20 (aver.=0.05)	0.00~0.12 (aver.=0.03)
FeO (range in wt%)	0.00~0.11	0.01~0.14	0.00~0.14
Mafic and accessary Ms	Bt, Amp, Ttn, Cal	Bt, Amp, Ttn, Hem, Cal, Chl	Bt, Amp, Ttn, (altered) Hem, Cal

* Numbers in parentheses show anlytical ones. **MP means microperthite. *** Ms means minerals. Bt=biotite, Rt=rutile, Cal=calcite, Chl=chlorite, Amp=amphible, Ttn=titanite and Hem=hematite.

They are anhedral except for the samples 9547 and 9546 which have subhedral Af grains. All the feldspars are variable in shape and size, and, especially in Af grains. Small Af grains are commonly scattered between and adjacently to larger feldspar grains in the samples 9539, 9547, 9646, 9536 and 9535. Porphyritic feldspar grains are distinctly observed in the samples, 9647 and 9546. In summary, these feldspar rock-textures are “mosaic” rather than hypidiomorphic.

Mineral assemblages in each rock type or in each unit are described in Kräutner & Bindea (1998) and Morogan et al., (2000). The mineral assemblages are shown in the bottom row of Table 1, except for felsic minerals. Amphibole is present in four samples (111, 9535, 9546 and 9539), and they are partially altered to secondary minerals such as calcite and hematite. Biotite is commonly present in the samples, and only biotite is present as a mafic mineral in the sample 129. Biotites completely altered to chlorite in the sample 9539, and partially altered to chlorite in the samples 9547, 9546, 9536 and 9535 from the same complex. Euhedral titanite is present in the four samples from the same complex. In addition, several hydrothermal alteration minerals are present. Zircon and apatite are commonly present as small accessory minerals in the samples, although they are not included in Table 1. The six samples except for the samples 111 are distinctly subsolvus rocks (Tuttle & Bowen, 1958). The true character of the apparently hypersolvus syenite 111 consisting solely of meso-microperthitic~anti-microperthitic grains is described in the Discussion section.

4. ANALYTICAL METHODS

Plagioclase was examined optically using a universal stage. Chemical compositions of minerals were obtained by a wavelength dispersive spectrometer (WDS) at an electron microprobe analyzers (EMPA): mainly with a JEOL JXA8800M and with a CAMEBAX. Rock textures and feldspar textures were mainly examined in microscopic scale using a petrographic microscope and a JEOL JXA8800M EMPA at Shiga University. The methods of quantitative and mapping analyses with a JXA8800M apparatus were already described in Nakano et al. (2014a, b, 2016). Mapping analyses were made by employing pixel numbers of 400×400. Oxide and silicate standards provided all by JEOL

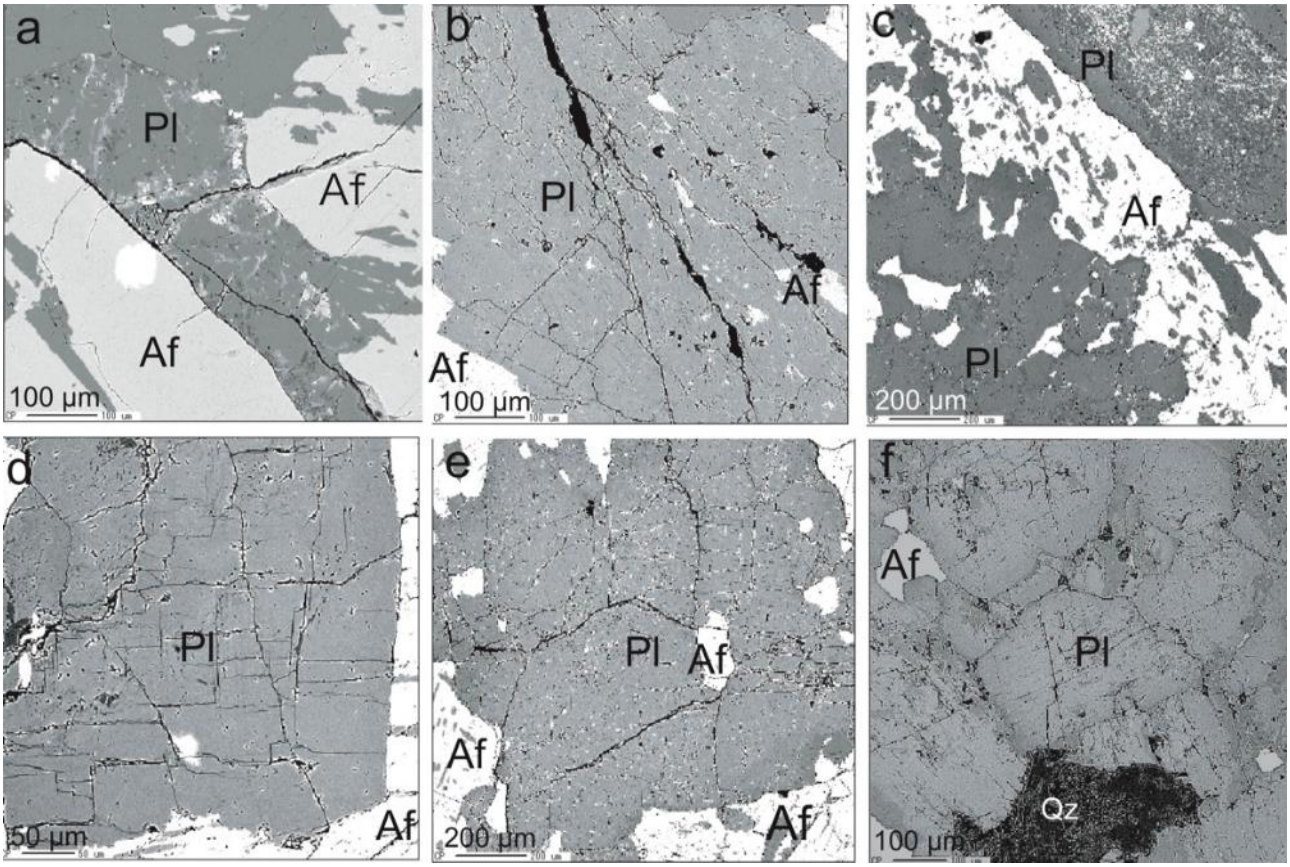

Figure 3. BSE maps showing occurrences of discrete plagioclase (Pl) grains with faintly and irregularly compositional zoning. (a) sample 129, (b) 9547, (c) 9539, (d) 9546, (e) 9536, and (e) 9535. Curved boundaries between plagioclase (Pl) and alkali feldspar (Af) grains are irregularly intricate. It is notable through the samples that Kf (K-feldspar) flakes of various shapes are scattered in Pl grains. In (a), (d) and (e), it is seen that Pl flakes of various irregular shapes are vice versa scattered in Afs adjacent to Pl grains. In (a), irregular fine Af veins are extended into Pl grains.

have been used for analyzed elements. We used for feldspars only total oxide compositions between 98% and 102% and within 1 % in the deviation of cation proportions of 5 based on O=8 according Nakano et al., (2016). EMPA analyses with a 5 μm beam yield phase compositions of minerals. Back-scattered electron images (**BSE** images in this paper) and secondary electron images (**SEI** images) were obtained by a FE-SEM, JSM-7600F, at Shinshu University in order to observe mainly fine cryptoperthitic textures. In addition, we made compositional analyses by an energy-dispersive spectrometer (EDS) attached at the FE-SEM. Obtained compositions were entirely the same as the above compositions obtained by the EPMA-WDS method. Cathodoluminescence (CL) images were obtained using a cold-cathode microscope (Luminoscope ELM-3R) at Okayama University of Science (Nakano et al., 2016), and CL spectra were obtained using CL apparatus with a photomultiplier (Hamamatsu) and a grating monochromator (Ritsu) attached to an EMPA at Shiga University.

5. FELDSPAR PETROGRAPHY

In all samples except for the mesoperthitic rock 111, Pl and Af grains are complicatedly intricate each other (Figs. 2, 3 and 4). As later shown, Pl grains in the samples are mostly consist of albite compositions so that they are named albite (Ab) in the text and labeled Ab in the figures. Af grains in the analyzed rocks commonly show microperthitic textures of constituent K-feldspar (Kf) and albite (Ab) (Fig. 4), both of which are mostly close to the end member compositions.

5.1. Plagioclase (albite)

Pl (albite) grains are wholly of irregular shapes with very irregular boundaries (Figs. 2B, 3 and 4). Irregular zoning patterns of plagioclases (Pls) are faint under a microscope and on BSE images (Figs. 3 and 4). The ranges of compositional variation are shown in Table 1. It is distinct in Ab grains that small Kf flakes of irregular shapes are commonly scattered through all the samples (Figs. 2, 3 and 4), and irregular veinlets of K-feldspars (Kfs) are sometimes developed from boundaries or cracks (Fig. 3a).

5.2. Alkali feldspar

Microperthitic (Afs) are also of irregular shapes with very irregular boundaries (Figs. 4, 5 and 6). It appears that they often penetrate and crosscut adjacent discrete Ab grains (Figs. 4 and 5). It is noted that small Kf grains with tartan twin textures (named "SC-Kf" in this paper), which are almost free of Pls and rather clear under microscope, are irregularly scattered (Fig. 5). Larger Af grains show microperthitic~meso-microperthitic textures with Ab inclusions of various shapes (roughly, patchy to lens-like or lamellae), and are that are more or less locally associated with turbidity and dirtiness (Figs. 3 and 5). It is remarkable that clear non-microperthitic areas are developed together with microperthitic areas in most of discrete Af grains. It is moreover noted that small Kf grains with SC-Kf, which are almost free of Pl inclusions and rather clear under microscope, are irregularly scattered (Fig. 5).

6. FELDSPAR MICROTEXTURES

The DAIC Af grains show a great variety of microperthitic textures totally different from any previous description of felsic rock microperthites. It is a result of our whole observations on the distinction of orientations of feldspar sections such as (001) or (010).

6.1. Mantle textures

In the DAIC Af grains, two-feldspar textures of core (Ab)–mantle (Kf) zoning is observed ("core-mantle" textures) through the samples except for 111 (Fig. 5), which are associated with lamellar or saw-tooth boundaries, and coexist with variable microperthitic textures. Core-like large Ab grains enclosed by Kfs are not necessarily located in the centers of individual grains and are sometimes located in rim areas. The core-mantle textures are comparable to "replacement microperthite" named by Alling (1938), and are like anti-rapakivi zoning (Nakano, 1992; Nakano & Suwa, 1995). And, associated microperthitic textures are similar to the "torn (microperthitic) textures" of Nakano et al., (2014a, b). The "torn texture" means that microperthitic Ab flakes appear to have been torn by resorption or dissolution from adjacent discrete large Ab grains.

6.2. Heterogenities of microperthitic textures

Textures of microperthites vary within a grain and grain by grain through the samples, which is summarized as three types of heterogeneity depending on the variations of constituent Ab characters (Figs. 4, 5 and 6): (1) size or width, (2) area proportion to Kf, and (3) shape (morphology).

(1) In the DAIC felsic rocks, microperthites and cryptoperthites of various widths coexist.

Microperthites have been generally known as optically visible or microscopic perthites, and cryptoperthites as optically invisible or TEM-order perthites (Smith, 1974; Smith & Brown, 1988). It is difficult to settle strictly the critical boundary width (Smith, 1974). In this study, we have recognized that the fine strings~films~lamellae (hereafter, lamellar) below 2~3 μm appear to be the same in texture, composition and interface property. Coarser constituent Abs are different from them as shown later.

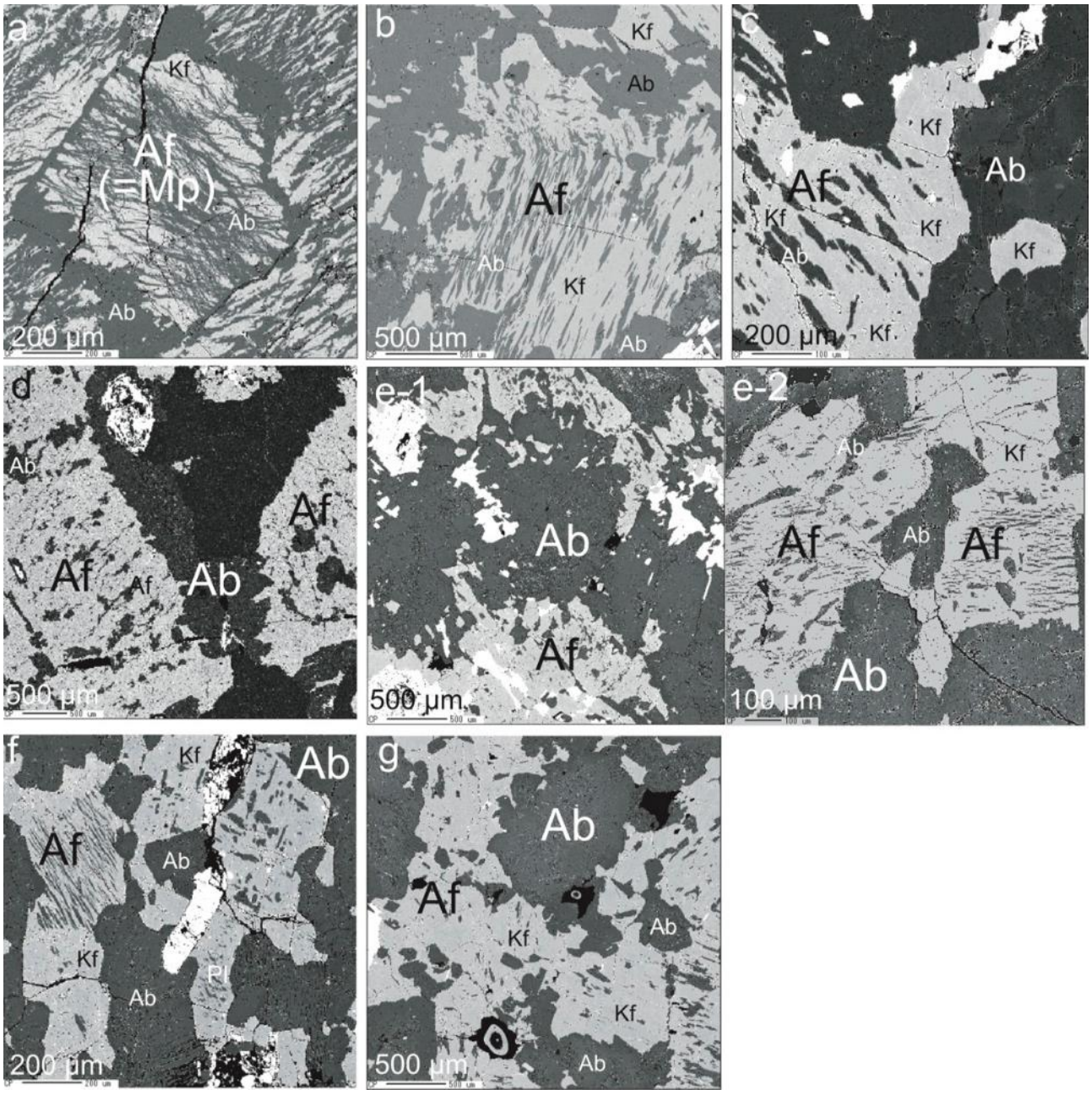

Figure 4. BSE images showing large heterogeneities of microperthitic textures. (a) sample 111 consisting only of meso-microperthite~anti-microperthitc (Mp) Af grains associated with intergranular albite (Ab) veins. K-feldspar (Kf) almost free of miroperthitic Ab are located here and there in a grain. (b) sample 129 showing meso-microperthitic Af and non-microperthitic Kf grains, which indicate complicated textural relations with Pl. Non-microperthitic Kf areas are also observed here and there in micrperthitic Af. (c) sample 9547 showing irregular distributions of Ab lenses and beads in host Kf. Textural relations between discrete Af and Ab grains are complicated. Non-microperthitic Kf areas are observed here and there. A small Kf grain is included in an adjacent Pl grain. (d) sample 9539 showing very irregular patch microperthitic two Af grains sandwich vein-like Ab grain with very intricate boundaries. (e)~(g): samples 9546~9535 showing nearly the same feldspar textures as the sample 9547 shown in (c). (a) = (001) section, (b) = roughly (001), (c) = (010), (d) = (010) (left Af) and (001) (right Af), (e) = roughly (001) (Afs), (f) = roughly (001) (Afs), (g) = (010) (Afs).

(2) The area proportions of constituent Abs are variable in a grain and grain by grain. Microperthitic (Af-dominant), meso-microperthitic (roughly equal Af and Pl) and anti-microperthitic (Pl-dominant) areas (Deer et al., 2001) coexist in various ways (Figs. 3 and 5), although anti-microperthitic areas are rarely observed. They are associated with non-microperthitic areas (Figs. 2 and 4) with comparable appearances to the SC-Kf grains (Fig. 5). The heterogeneity of this type was observed in the six samples except for the 111 only of mesoperthitic Af grains. Meso-microperthitic areas in the six samples are often observed around larger Pls patches as described above (Figs. 5a-2, b-2 and c-2). In the sample 129 among the six samples, Af grains are often of meso-microperthites (Fig. 4). Anti-microperthitic textures are sometimes locally developed only in the sample 111 (Fig. 4a). The other five rocks consist dominantly of microperthitic areas with variable distribution patterns of the other textural areas (Figs. 4 and 5).

(3) The DAIC microperthites show a diversity of constituent Ab morphology (Fig. 6). Microperthite constituent Abs coarser than 2~3 μm with shapes other than lamellar are bead, rod and string, lens and so on (Smith & Brown, 1988). For much larger-scale microperthitic Abs, two types of patches are distinguished: Type I is rather clear and of rather regulated, box-like patchy shapes on both the (001) and (010) sections, and Type II is turbid and of irregular shapes like patch microperthites in granitic rocks described to date (e.g., Lee & Parsons, 1997; Hashimoto et al., 2005a, b). The type II patches are often bordered by cracks from Or-rich feldspars. The aforementioned "torn" Ab grains are of the type II, which suggests that most of the type II patches are of the same origin. The vein-like microperthites in sections, which are observed especially in the sample 129, appear to be three-dimensionally curved large lenses.

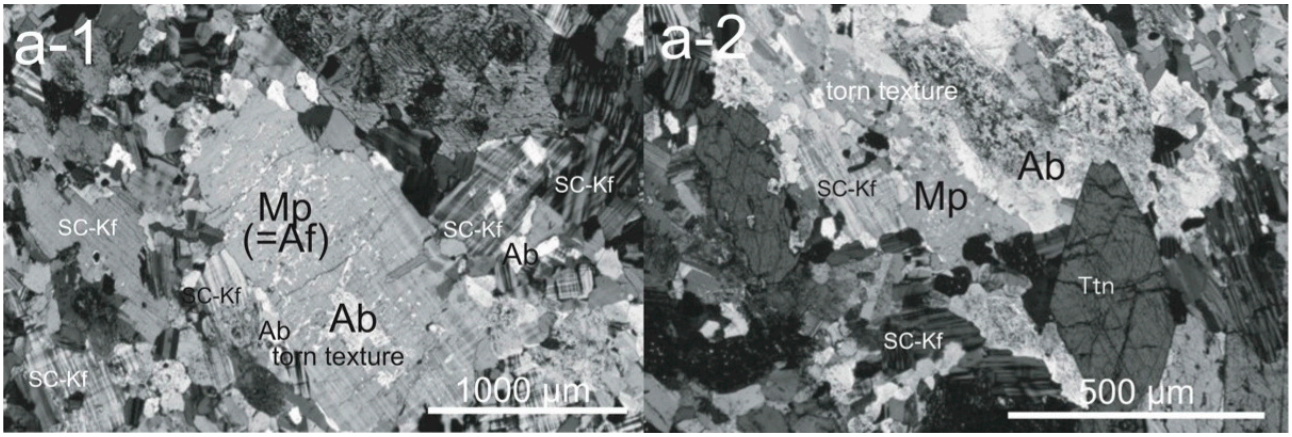

Figure 5 (a-1~a-2). Photomicrographs under crossed nicols showing representative core-mantle textures associated with "torn textures" showing microperthitic~meso-microperthitic (Mp) textures in individual Afs. Non-microperthitic Kf areas are more less present. These textures are commonly observed in the samples including sample 9539 except for samples 111 and 129 consisting dominantly of microperthitic Afs (Mps). In addition, small clear tartan twinned Kf grains with no or few small microperthitic Ab (SC-Kf) are present here and there through the samples except for the sample 111. (a) sample 9547=(001)

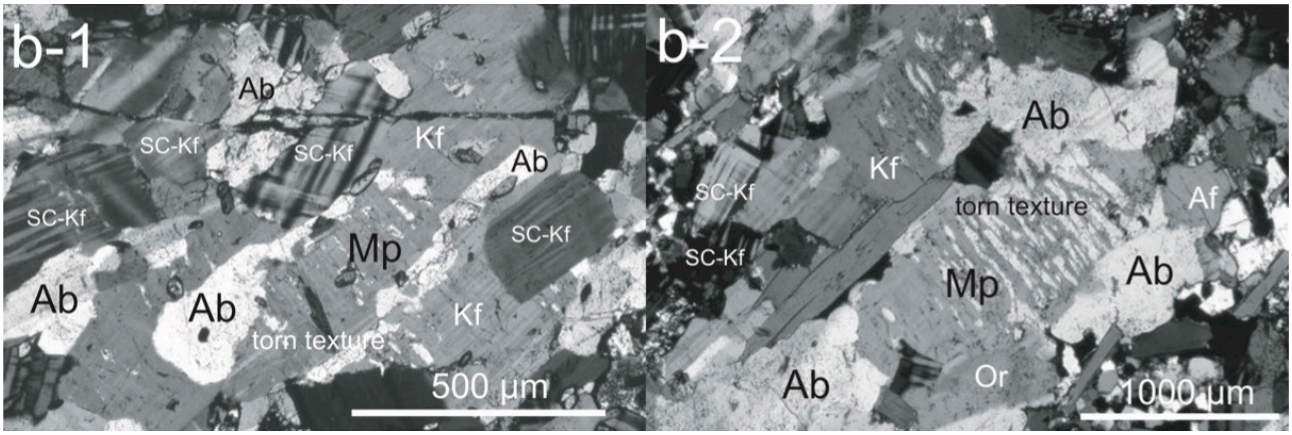

Figure 5 (b-1~b-2). 9546 = inclined (001)

Other than the above textural types, braided patterns of elongated Abs along two different orientations are often observed on (001) sections in the DAIC Afs, some of which are similar both to braid microperthites of Goldich & Kinser (1938) and those of Barth (1969) and Ramberg (1972). Interlocking or interpenetrating microperthites described by Alling (1938) are also distinctly present on both (001) and (010) sections. Flame microperthites as described by Pryer & Robin (1995) and Vernon (1999), whose Ab-rich feldspars may be actually broad lenses developed from rims, were also observed distinctly in some of the samples.

6.2.1. Dominant types in the individual rocks

(1) Sample 111 from the Complex of muscovitized syenites: Meso-microperthite and anti-microperthites are extensively developed through all the grains (Figs. 2B-a and 4a). All the grains are associated with intergranular Ab veins, which are connected to microperthitic Ab lamellae inside the Afs. Interlocking textures are distinct. The textures are apparently comparable to those in granulites or granulite-facies rocks and gneisses (Yund & Ackermand, 1979; Hayob et al., 1989; Voll et al., 1994; Rasse, 1998; Yoshimura et al., 2000; Hokada, 2001), those in hypersolvus syenites or monzonites (Fuhrman et al., 1988; Oba et al., 1997), those in granites (Day & Brown, 1980).

(2) Samples 129 and 9547 from the Complex of nepheline syenites: In the sample 129, meso-microperthitic areas are notable (Figs. 4b and 6e, f), and flame microperthites are developed with braid textures and interlocking microperthites. Ab veins and patches of the type II are there crosscut by Kfs. Inside such patches, vice versa, there are often small Kf flakes, these microperthites are not so turbid under microscope. In contrast, the Af textures of the sample 9547 are basically common to the three samples 9546, 9536 and 9535 described below, although it is finer grained as and extensively foliated.

(3) Sample 9539 from the Complex of granitic rocks: Although the microperthitic textures are partly similar to those of granite microperthites (e.g., Hashimoto et al., 2005a), (Fig. 4d), many textural features common to the other samples are also present, which are not common to ordinary granite microperthits. Crosscut relationships between hydrothermally formed patch microperhites and optically visible fine (cyptoperthitic) lamellae, which record hydrothermal perthite coarsening, were not observed.

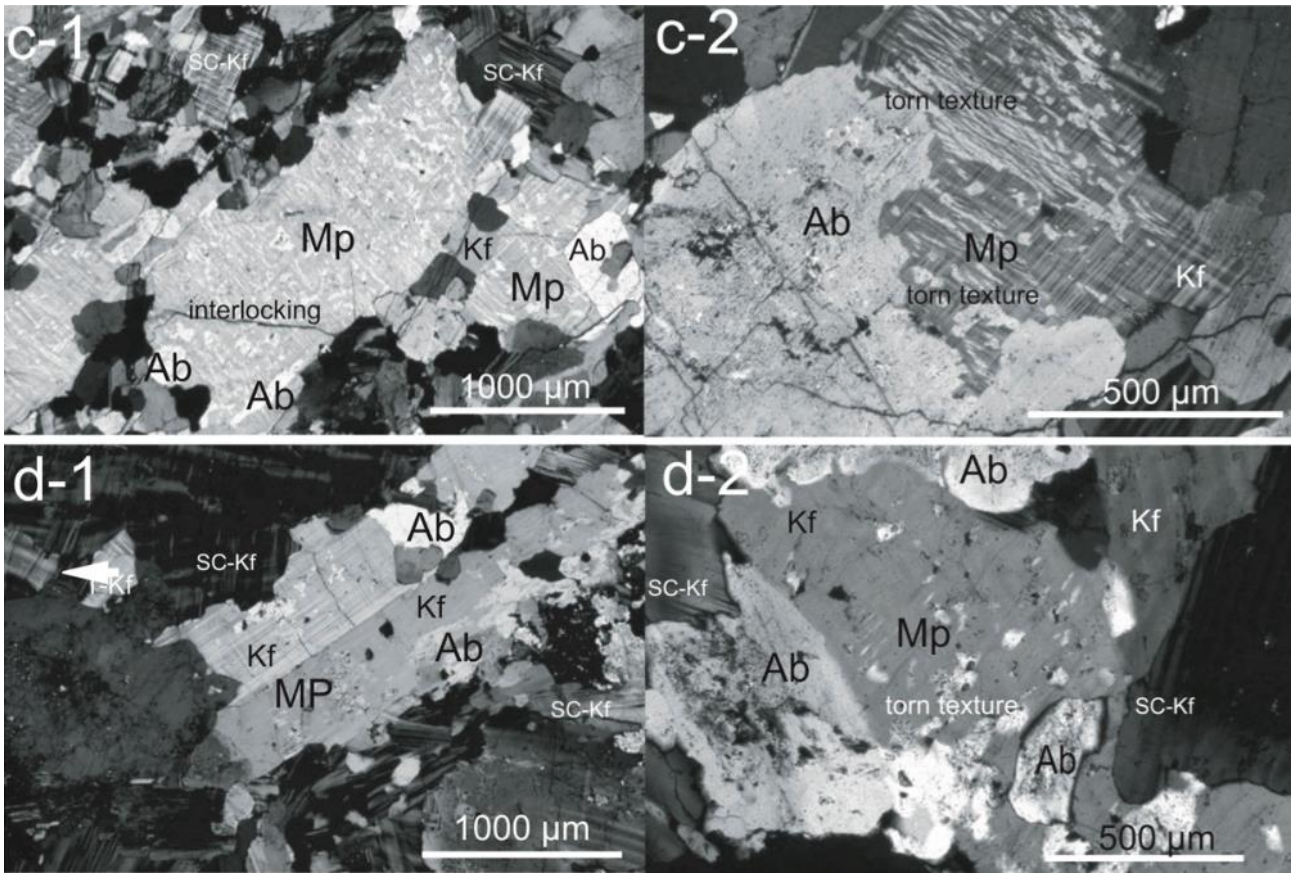

Figure 5 (c-1~d-2). 9536 = inclined (001) and (d) 9535 = (010), which correspond to each porphyritic or large Afs showing the above textures nearly in the center of each photomicrograph.

(4) Samples 9546, 9636, and 9535 from the Monzonite-syenite complex. The principal features of microperthites are nearly the same in all the three rocks, which are also common to those of the sample 9547. Core-mantle zoning (Figs. 5 and 6d) is common. Adjacently to discrete Ab grains, small microperthitic Ab patches with irregular shapes (Fig. 5) appear to be torn from them. In most of such cases, discrete Ab grains appear to be vice versa invaded or crosscut by Kfs. In addition, flame (plume) microperthites are developed from grain boundaries as shown in Fig. 6c, and flames often show a zigzag or wavy patterns (Fig. 6d, e). These are common also to the sample 129.

6.3. Cryptoperthites

Af textures were observed using a FE-SEM. The FE-SEM resolves cryptoperthites with widths at least of 100 nm, probably close to 50 nm, as shown in Fig. 2c-3 of Nakano et al., (2016). If according to the aforementioned general definition of cryptoperthites,

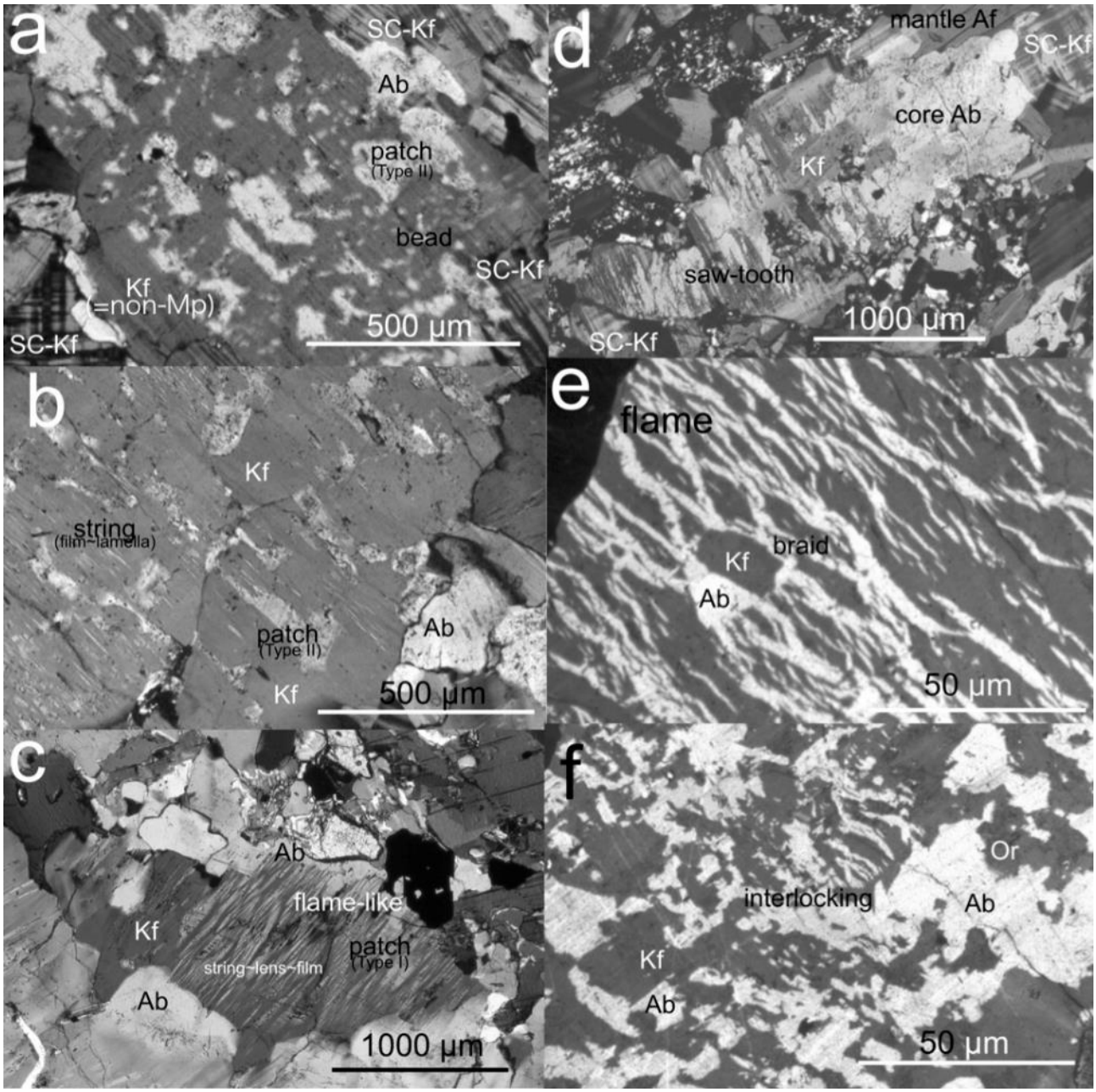

Figure 6. Photomicrographs under crossed nicols showing typical types of microperthites (Mp). Textures showing replacement or coarsening of fine Ab films or lamellae by turbid Ab patches are not observed. Several types of Mp generally coexsist in a Af grain. Types of (a)~(f) are more or less commonly present through the samples, although braid texture of (e) is especially developed in samples 111 and 129, and interlocking texture of (f) in sample 129. (a) sample 9546 = (001), (b) sample 9535 = (010), (c) the sample 9536 = (001), (d) sample 9547 = (001), (e) sample 129 = (001), and (f) sample 129 = (001).

it is said that cryptoperthites are more or less present commonly in the samples. In the above resolution level, however, the present FE-SEM observations show that there is no cryptoperthite below 1 μm in width in the five samples 111, 129, 9547, 9546 and 9535, but are present only in samples 9539 and 9536

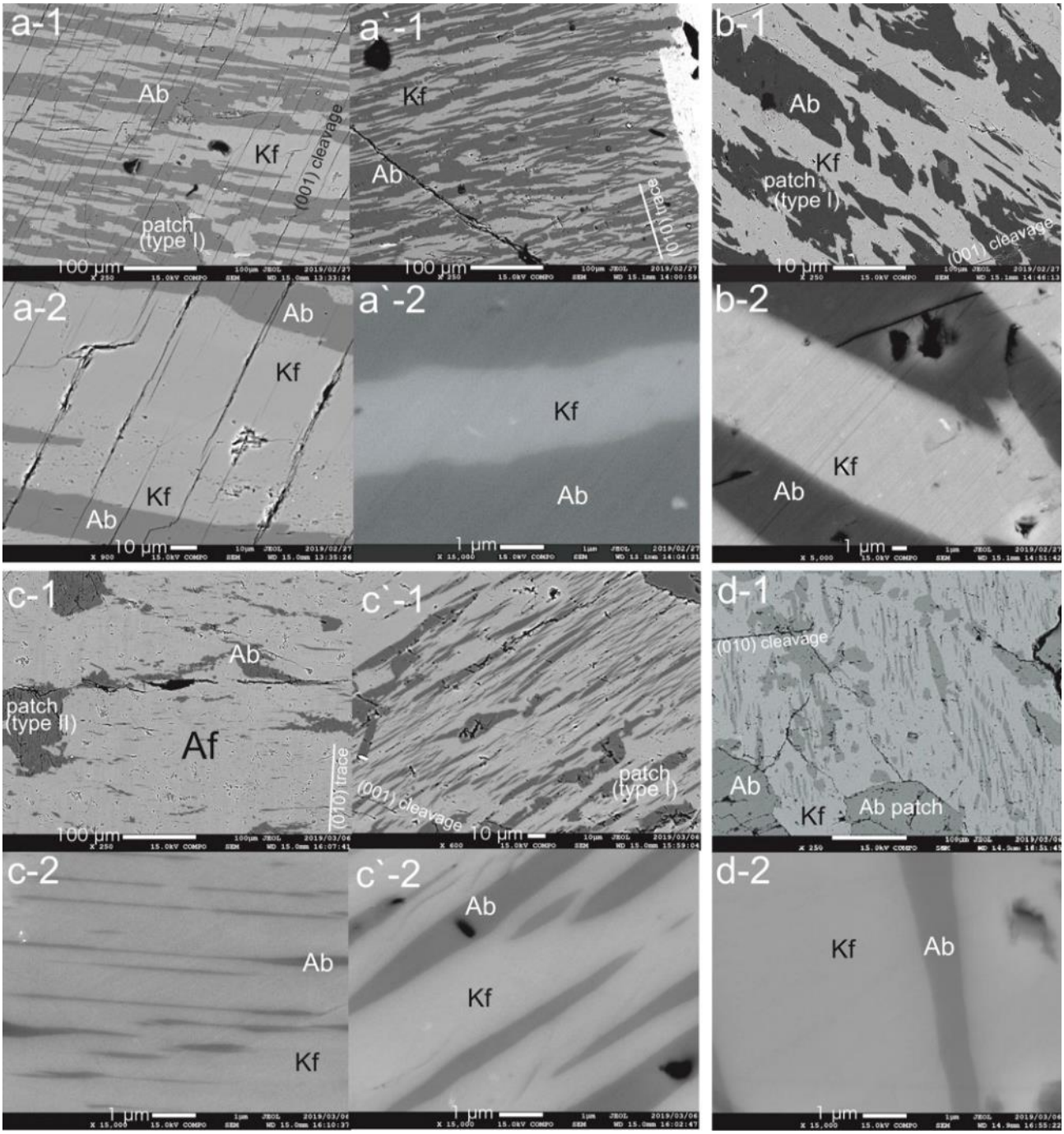

Figure 7 (a-1~d-1). FE-SEM BSE images showing cryptoperthitic~microperthitic textures. (a) and (a') sample 111, (a) = (010) section with distinct (001) cleavages showing meso-microperthitic texture of film or lense and patch (type I) types, (a') = (001) with distinct (001) cleavages showing braid texture of curving or bending Ab films, (b-1) sample 129 = (010) showing small Ab dots (small beads)~string~lens~patch (type I) microperthitic textures with small beads, where large lenses or paches appear to be invaded and separated by Kf, (b-2) shows an enlarged part in the same Af grain of (b-1), two constituent feldspars of which are associated with large pores. (c) and (c') sample 9539, (c) = (001) showing turbid patch (type II) microperthitic textures with curved and undulated fine Ab strings, no micropore in (c-2), (c') = (010) showing string~lens~lamella~film~patch (type I) microperthites, no micropore in Kf and one micropore in three Ab lenses or lamellae in (c'-2). (d) sample 9536 = inclined (001), (d-1) showing coexsiting of Ab beads, rods, lamellae or films, lenses and patches (types I and II), large type II patches are associated with many micropores but type I patches are with much lesser micropores, irregular cracks are developed especially around type II patches, (d-2) showing clear Ab lamellale of 1 μm in width and clear Kf host.

(Fig. 7). In the granite sample 9539, there are very fine lamellar, optically invisible cryptoperthites around 100 nm (or less) in width (Fig. 7). In the syenite sample 9535, there are cryptoperthites of widths around several hundred nm that are not so fine as in the granite sample 9539. In the remaining five samples, the narrowest widths of Ab strings are commonly above 1 μm. These cryptoperthite and string microperthite around several microns are mostly clear without turbidity as seen in Fig. 7. These cryptoperthitic~fine-microperthitic textures are very similar to those in deformed rocks from SW Amazonia (Tohver et al., 2005) and in felsic granulites from the Bohemian Massif (Tajčmanová et al., 2012).

It should be noted in these samples, as already mentioned, that there is no evidence showing both that turbid Ab patches cut across cryptoperthitic lamellae or microperthitic film (lamellae) and that small turbid patches are developed on pristine cryptoperthitic and microperthitic lamellae.

6.4. Turbidity

Hydrothermal patch microperthites in granites are associated with turbidity (turbid patch microperthites) (Nakano et al., 2019). Turbidity under a microscope is due to the presence of abundant micropores (Worden et al., 1990; Guthrie & Veblen, 1991; Walker et al., 1995). Turbidity is partly observed especially in the syenite sample 111 and granite sample 9539 with “dirtiness” under a microscope. “Dirtiness” is a microscopic appearance for larger, spotted micropores and inclusions, which was found in the Kakkonda & O’hara granodiorite Afs (Nakano et al., 2014a, b). However, Kfs as a microperthitic dominant constituent in the remaining five samples are much clearer than in granite microperthites under a microscope, and, in the nepheline syenite 129, turbidity or dirtiness is very limited. Summarizing, (1) SC-Kf grains are especially clear due to few micropores (Figs. 4 and 5), (2) non-microperthitic Kf areas are relatively clear, too (Figs. 3, 4 and 5), (3) constituent fine Abs up to ca. 10 μm are rather clear, and (4) Ab patches of the type I are not so turbid with few micropores (Fig. 7).

7. FELDSPAR CHEMISTRY

7.1. Local bulk and bulk compositions of Afs with a 50 μm beam

Average compositions were obtained from representative textures in individual samples as follows (Table 1): those of the sample 111 with meso-microperthites and the sample 129 dominantly with meso-microperthites are intermediate in the Or-Ab series, and those of the remaining five samples are Or-rich. Table 1 shows that An contents in the obtained average compositions are commonly around 1 mo% through the seven samples, so that the DAIC Afs are practically recognized to be Or-Ab binary feldspars.

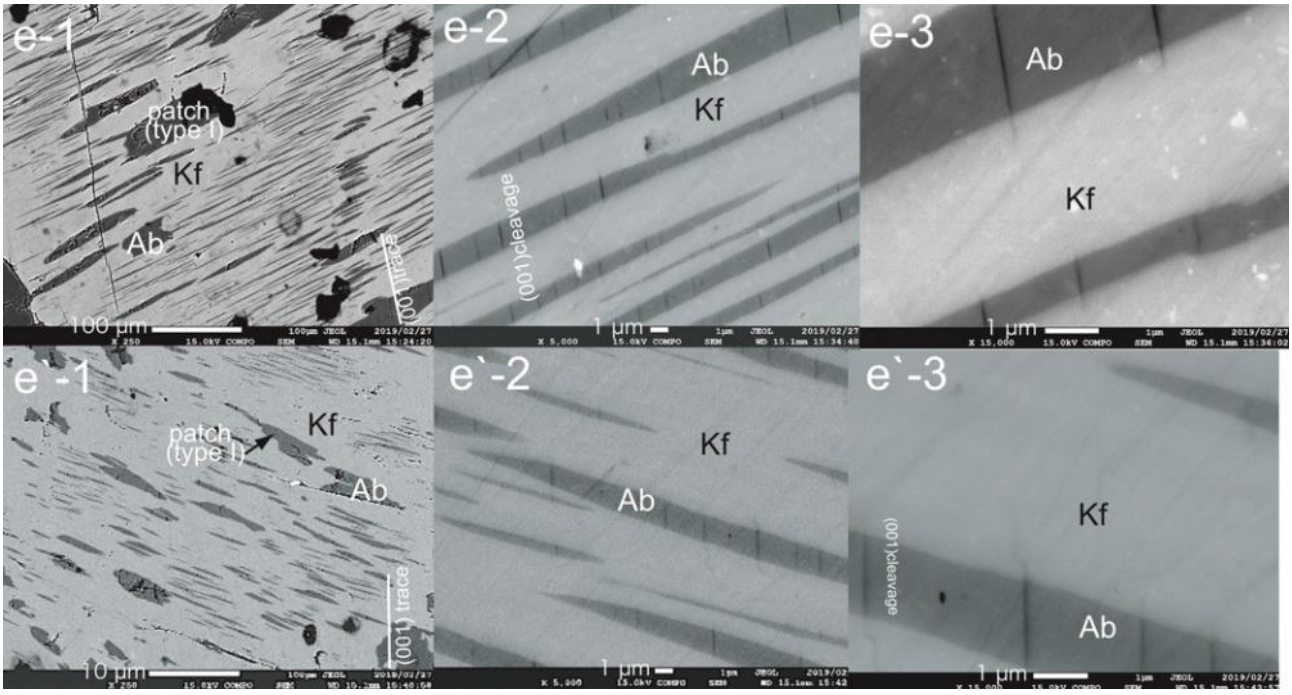

Figure 7 (e-1~e’-3) sample 9535 = (010) showing clear Ab fine-lamellae~films~lenses~patches of type I and clear Kf host without macropores, (e-2) ~ (e-3) and (e’-2) ~ (e’-3) showing fine Ab lamellae free of micropores but with distinct (001) cleavages and clear Kf host without micropores

7.2. Compositions obtained by EMPA analyses whith a 5 μm beam

7.2.1. Plagioclases

Obtained Pl compositions are shown in Table 1. The variation ranges of Pl compositions are very narrow through the all samples. The DAIC Pls are practically recognized to be An-Ab binary series due to low Or contents. In the samples 111 and 129, almost all Pl compositions are close to the end-member Ab. Exceptionally, only one Ab-rich oligoclase composition was obtained in the sample 111 and three andesine compositions were obtained in the sample 129. These compositions are remnant, escaped from albitization. Pl compositions of the samples 9547 and 9539 are not so extreme as in the above syenites sample 111 and 129, but are in the short compositional range of Ab. In the remaining three samples, 9546, 9536, and 9535, they are variable in the range from oligoclase to Ab (Table 1), but most of them are in the range of Ab with weak zoning. These results are consistent with Bindea, (1993, 2010) and Morogan et al., (2000), both of who reported the dominant proportion of Ab in the DAIC Pls, and with Pál-Molnár et al., (2015b) who described the examined Pls in the granites dominantly as Ab.

7.2.2. Alkali feldspars (microperthites)

The compositional features of two constituent Ab-rich and Or-rich feldspars are summarized in Table 1 and Figs. 8 and 9. The representative chemical compositions of both the Or-rich and Ab-rich feldspars in the microperthites are shown in Table 2. In addition, concrete local compositional pairs in the microperthites from the selected four samples are individually shown in Figure 8.

The compositional variation ranges of microperthitic Or-rich feldspars in the samples are very small (Fig. 8). Extreme compositions reach to $Or_{96.5\sim98.6}$ in the individual samples (Fig. 8), and most of the compositions are around 95 mol% Or (Tables 1 and Fig. 8). These results are consistent with the results by Pál-Molnár et al., (2015b) that microperthitic Or-rich feldspars in the granites are

Table 2. Selected, representative compositions of microperthitic constituent feldspars in the DAIC felsic rocks.

	111		129		9547		9539		9546		9536		9535	
	Or-rich	Ab-rich	Or-rich	Ab-rich	Or-rich	Ab-rich	Or-rich	Ab-rich	Or-rich	Ab-rich	Or-rich	Ab-rich	Or-rich	Ab-rich
SiO2	63,45	68,20	63,70	68,44	64,08	69,38	64,07	68,37	63,87	64,46	63,21	64,54	63,57	63,80
Al2O3	17,58	19,99	18,41	20,09	18,34	19,27	17,79	19,50	17,76	21,83	18,44	21,49	18,51	22,27
FeO	0,08	0,10	0,04	0,02	0,03	0,12	0,05	0,03	0,00	0,03	0,07	0,08	0,04	0,01
CaO	0,01	0,08	0,00	0,02	0,01	0,16	0,03	0,18	0,00	2,84	0,06	2,59	0,00	3,10
Na2O	0,30	11,57	0,67	11,70	0,44	11,64	0,30	11,48	0,48	9,97	0,53	9,99	0,29	9,85
K2O	16,58	0,04	16,12	0,04	16,21	0,10	16,58	0,16	16,21	0,07	15,55	0,07	16,13	0,06
BaO	0,00	0,03	0,10	0,04	0,76	0,00	0,12	0,06	0,67	0,01	0,72	0,04	0,77	0,00
Total	98,00	100,0	99,04	100,3	99,87	100,7	98,93	99,78	98,99	99,22	98,57	98,80	99,30	99,10
	Atomic proportions on the basis of O=8													
Si	3,005	2,979	2,981	2,979	2,986	3,009	3,005	2,994	3,002	2,860	2,977	2,874	2,978	2,837
Al	0,981	1,029	1,016	1,031	1,007	0,985	0,983	1,007	0,984	1,142	1,024	1,128	1,022	1,167
Fe	0,003	0,004	0,002	0,001	0,001	0,004	0,002	0,001	0,000	0,001	0,003	0,003	0,001	0,001
Ca	0,001	0,004	0,000	0,001	0,000	0,008	0,001	0,008	0,000	0,135	0,003	0,124	0,000	0,148
Na	0,027	0,980	0,061	0,987	0,040	0,979	0,027	0,974	0,044	0,858	0,048	0,863	0,026	0,849
K	1,002	0,002	0,963	0,002	0,963	0,006	0,992	0,009	0,972	0,004	0,935	0,004	0,964	0,004
Ba	0,000	0,001	0,002	0,001	0,014	0,000	0,002	0,001	0,012	0,000	0,013	0,001	0,014	0,000
Total	5,019	4,998	5,023	5,001	5,012	4,990	5,013	4,995	5,014	5,000	5,002	4,996	5,006	5,006
	Or-Ab-An ternary compositions													
An	0,0	0,4	0,0	0,1	0,0	0,8	0,1	0,8	0,0	13,6	0,3	12,5	0,0	14,8
Ab	2,7	99,4	5,9	99,7	4,0	98,7	2,6	98,2	4,3	86,0	4,9	87,1	2,7	84,9
Or	97,3	0,2	94,1	0,2	96,0	0,6	97,2	0,9	95,7	0,4	94,8	0,4	97,3	0,4

$Or_{94\text{-}97}$. Anorthite (An) contents are low (below 0.1 mol%) with few exceptions (Tables 1 and 2). The host Or-rich feldspars are practically potassium feldspar (Kf), and are low-microcline of Kf (hereafter, LMKf). For the LMKf, we detected characteristic patterns of compositional variations with small compositional variations (Fig. 10): namely, in dominant Or-rich feldspars (Kf-1), much Or-richer feldspars closer to the end member composition (Kf-2) are present as bands, veins and streaks. Such Kf-2 elongations are dominantly of two orientations: one is roughly along the a-axis and another one is roughly along the b-axis (Fig. 10a~d). In Fig. 10e-2, it appears that a bundle of Kf-2 streaks penetrate or infiltrate Kf-1 parts. The present occurrences of the Kf-2 have not been reported hitherto.

The compositional variation ranges of microperthitic Abs in the samples are also narrow (Fig. 8). Most of the compositions are close to the end-member Ab, although their ranges of variation ranges are larger than those of Or-rich feldspars (Fig. 8). The extreme composition of the microperthitic Abs is 99.7 mol% Ab or 99.8 mol% Ab (Fig. 9a-3) in sample 129. In the samples 111 and 129, almost all Ab compositions are close to the end member Ab. Ab compositions in samples 9547 and 9539 are in the range from $Ab_{94.6}$ to $Ab_{99.3}$ and from $Ab_{91.5}$ to $Ab_{98.5}$, respectively. In the remaining three samples 9546, 9536 and 9535, compositional variations are in the range of albite~oligoclase above Ab_{80} (Fig. 8).

It is noted here that the extreme Ab composition is not paired with the extreme LMKf composition in each sample. Figure 9 concretely shows such disequilibrium compositional pairs.

7.2.3. BaO and FeO contents in microperthites

Barium is richer in LMKfs than in Abs in the DAIC microperthites (Tables 1 and 2). The BaO contents in the constituent two feldspars vary irregularly in all the samples. The maximum BaO contents in LMKfs are not so high throughout the sample except for 1.94 wt% in sample 9536. Any relationship between BaO and other oxide component such as K_2O is not recognized. The contents of FeO are very low in the microperthites (Tables 1 and 2).

8. CL EMISSIONS FROM THE FELDSPARS

All the LMKfs are blue or greenish blue under the luminoscope, and all the Abs are red, some of which are white due to saturated strong emissions (Fig. 11a~d). The representative spectra both of LMKfs and Abs in the selected two samples 129 and 9535 are shown in Fig. 11e, f. Both spectra of LMKfs commonly consist of an asymmetric, strong, broad

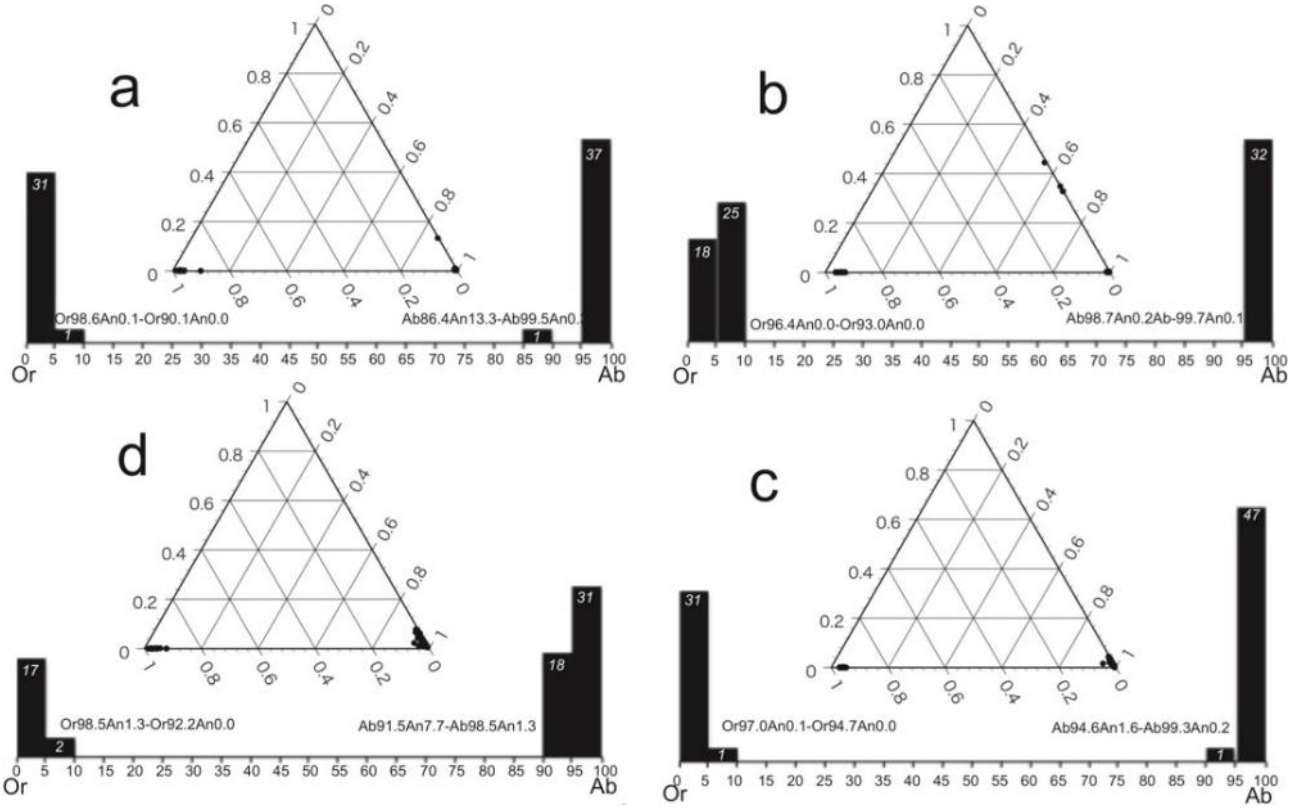

Figure 8 (a~c). Obtained compositions of microperthitic two feldspars in the analyzed samples are individually shown in each set of Or-Ab binary bar graphs and Or-Ab-An ternary diagrams. White numbers in the upper part in each bar show numbers of obtained compositions.

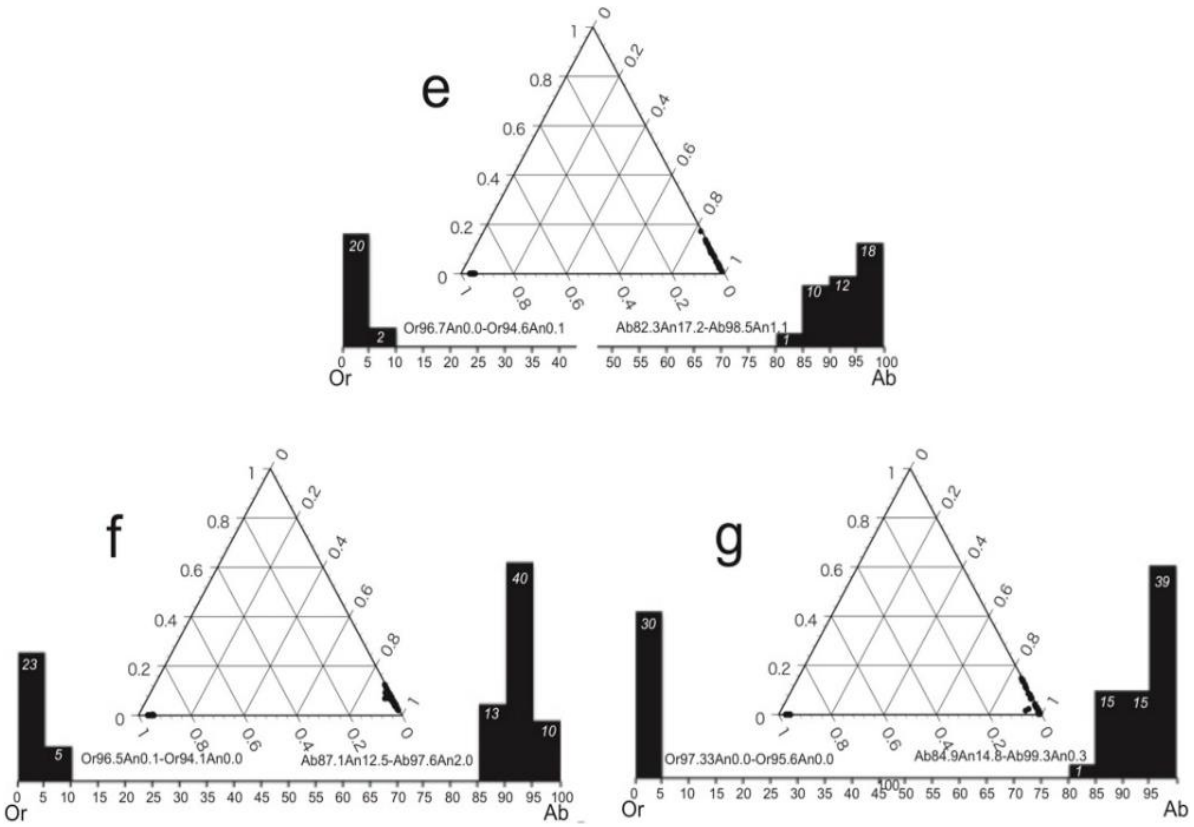

Figure 8 (e~g). Obtained compositions of microperthitic two feldspars in the analyzed samples are individually shown in each set of Or-Ab binary bar graphs and Or-Ab-An ternary diagrams. White numbers in the upper part in each bar show numbers of obtained compositions.

peak in the range of 400-500 nm and an asymmetric, moderate, broad peak in the range of 700-800 nm. In contrast, both spectra of Abs commonly consist of a relatively weak, broad peak in the blue range and a slightly weak peak in the red range.

The blue-emissions consist of several peaks caused by several different factors such as Al-O defects, Ti impurity, and other lattice defects (Finch & Klein, 1999; Lee et al., 2007; Kayama et al., 2010). The red CL emissions of the DAIC Abs are considered to be due to the presence of Fe^{3+}. These CL characters of the feldspars are different from those in hypersolvus syenites undergone partial replacement reactions catalyzed by H_2O forming low-temperature patch perthites (Finch & Klein, 1999; Nakano et al., 2005; Lee et al., 2007; Kayama et al., 2010). In contrast, they may be comparable to those of microperthitic feldspars in granite pegmatites (Sánchez-Muñoz et al., 2006), in which blue emissions of variable intensities arise in host Or-rich feldspars, and red emissions in guest Ab-rich feldspars.

9. CHEMISTRY OF COEXISTING MINERALS

9.1. Biotite

Biotite is the most common mafic mineral in the examined rock samples. The chemical compositions of biotites that are present in the samples are shown in Table 3. The DAIC biotites are mosly fresh, except for the granite sample 9539 in which biotite is completely altered to chlorite (Table 1). The DAIC biotites are annites with high-Ti contents. The present biotite compositions are comparable to those in the syenite and monzodiorites reported by Morogan et al. (2000) and in syenites and granitoids by Pál-Molnár et al. (2015a). The compositions show a successive variation trend toward Fe-rich and Mg-poor ones in the order of 9535, 9536, 9546, 9547, 129 and 111, which is consistent with the succession of the geological units.

9.2. Amphibole

The chemical compositions of the present amphiboles are shown in Table 3, which are consistent with those in Morogan et al., (2000). Compositionally the amphiboles are calcic amphiboles varying from ferro-edenite to ferro-hornblende (Leake et al. 1997). Morogan et al., (2000) pointed out that the amphibole compositions are comparable to those from silica-undersaturated rocks.

9.3. Titanite

The chemical compositions of the present titanites shown in Table 3 are consistent with those in Morogan et al., (2000).

Table 3. Representative chemical compositions of biotites, amphiboles and titanites in the seven DAIC felsic rocks.

	Biotite											
Wt%	111		129		9547		9546		9536		9536	
SiO_2	35,67	35,19	35,14	33,92	34,75	34,36	34,99	35,53	36,08	35,64	34,14	35,75
TiO_2	3,92	3,54	3,75	2,95	1,96	0,90	2,50	1,29	1,35	1,17	1,92	0,76
Al_2O_3	13,03	12,32	12,99	14,25	14,14	16,71	14,42	14,65	15,27	15,55	15,63	14,47
FeO	26,78	27,16	26,06	27,65	25,59	23,48	23,54	23,66	21,70	21,94	23,56	21,98
MnO	0,73	0,62	0,60	0,48	1,74	1,68	0,73	0,73	1,33	1,28	1,08	1,12
MgO	5,07	5,27	6,40	4,97	7,75	7,65	8,26	8,62	10,15	9,71	6,73	10,07
CaO	0,00	0,00	0,00	0,00	0,00	0,36	0,00	0,01	0,08	0,14	0,13	0,03
Na_2O	0,19	0,17	0,07	0,12	0,09	0,14	0,03	0,09	0,09	0,03	0,07	0,09
K_2O	9,63	9,98	9,77	9,59	10,05	8,70	10,10	10,03	9,78	8,59	9,53	9,93
Total	95,02	94,25	94,78	93,92	96,07	93,97	94,56	94,60	95,83	94,04	92,79	94,19
	Atomic proportions of cations on the basis of O=22											
Si	5,722	5,731	5,642	5,542	5,525	5,472	5,565	5,638	5,589	5,597	5,533	5,657
Al	0,472	0,433	0,453	0,362	0,234	0,108	0,299	0,154	0,157	0,138	0,234	0,091
Ti	2,463	2,364	2,458	2,744	2,650	3,136	2,704	2,740	2,788	2,878	2,986	2,699
Fe	3,593	3,699	3,499	3,779	3,403	3,127	3,131	3,140	2,812	2,882	3,193	2,909
Mn	0,099	0,085	0,081	0,067	0,234	0,226	0,098	0,097	0,175	0,170	0,149	0,150
Mg	1,212	1,279	1,532	1,211	1,836	1,816	1,959	2,039	2,345	2,274	1,626	2,376
Ca	0,000	0,000	0,000	0,000	0,000	0,062	0,000	0,002	0,013	0,023	0,023	0,005
Na	0,058	0,053	0,023	0,037	0,028	0,042	0,008	0,026	0,026	0,009	0,022	0,027
K	1,971	2,073	2,001	1,999	2,038	1,767	2,049	2,031	1,933	1,721	1,971	2,004
Total	15,589	15,717	15,688	15,742	15,949	15,756	15,813	15,867	15,839	15,691	15,737	15,918

	Amphibole						Titanite			
Wt%	9547		9536		9535		9547	9536	9535	9546
SiO_2	37,63	38,12	38,38	39,40	38,71	38,52	29,53	29,54	32,22	30,75
TiO_2	0,73	1,05	0,92	2,64	2,76	2,84	35,13	35,78	36,46	34,89
Al_2O_3	11,08	11,82	10,72	10,79	11,36	11,34	1,44	1,80	1,78	2,50
FeO	27,55	26,18	24,51	21,71	22,01	22,10	1,94	1,73	1,07	1,55
MnO	1,41	1,44	1,35	0,88	1,03	1,04	0,15	0,07	0,04	0,08
MgO	3,96	3,97	5,88	5,72	5,44	5,74	0,02	0,03	0,00	0,01
CaO	8,08	8,21	9,12	9,49	9,62	10,15	26,05	26,16	26,87	26,71
Na_2O	3,95	3,48	3,43	3,23	2,88	3,36	0,16	0,09	0,00	0,01
K_2O	1,93	2,15	1,89	1,87	1,82	1,84	0,00	0,00	0,03	0,06
Total	96,29	96,41	96,20	95,73	95,63	96,91	94,42	95,19	98,48	96,54
	Atomic proportions of cations on the basis of O=23						O=4			
Si	6,013	6,053	6,077	6,282	6,171	6,112	1,023	1,014	1,059	1,036
Al	2,086	2,211	2,000	2,027	2,134	2,121	0,916	0,923	0,901	0,884
Ti	0,087	0,125	0,110	0,317	0,330	0,338	0,059	0,073	0,069	0,099
Fe^{3+}	1,329	1,131	1,098	0,153	0,316	0,121	0,056	0,050	0,030	0,044
Fe^{2+}	2,352	2,345	2,148	2,742	2,618	2,811				
Mn	0,190	0,194	0,181	0,119	0,139	0,140	0,004	0,002	0,001	0,002
Mg	0,942	0,	1,387	1,359	1,292	1,356	0,001	0,002	0,000	0,001
Ca	1,384	1,397	1,547	1,622	1,643	1,726	0,967	0,962	0,946	0,964
Na	1,223	1,072	1,053	0,998	0,891	1,034	0,011	0,006	0,000	0,000
K	0,393	0,434	0,382	0,380	0,371	0,372	0,000	0,000	0,001	0,003
Total	16,000	15,904	15,982	15,999	15,904	16,131	3,037	3,030	3,007	3,032

10. DISCUSSION

10.1. Magmatic crystalization

Morogan et al., (2000) estimated the crystallization temperature of ca. 870°C for the DAIC syenite and the temperature of ca. 720°C for the quartz syenite. However, they mentioned that the DAIC feldspar crystallization appears to have terminated under subsolvus conditions from the feldspar compositions. Fall et al., (2007) described for the nepheline syenites that fluid inclusions in nepheline, aegirine and Ab were trapped at magmatic conditions on or below the H_2O-saturated nepheline syenite solidus at about 400-600°C and 2.5-5 kbars. This lower temperature may be plausible in the presence of abundant volatile components lowering the solidus.

Magmatic feldspar crystallization temperatures are estimated using feldspar compositions on the basis of the Or-Ab-An ternary feldspar phase relations (Fuhrman & Lindsley, 1988; Wen & Nekvasil, 1994), although feldspar phase relations are still uncertain especially in the low temperature regions. Temperatures in approximately of 500-400°C range were obtained using pairs of Pl compositions and Af average compositions shown in Table 1 (P=2kb), although the pairs do not lie on any isotherm, and those of the samples 111 and 9536 did not permit calculations. The obtained temperatures are probably of later low-temperature disequilibrium reorganization. The andesine in the sample 129 may be of primary Pl crystallized at higher-temperatures at least above 600°C.

10.2. Magmatic reactions

Core-mantle textures with lamellar or saw-tooth boundaries are common through the DAIC felsic rocks except for sample 111 (Fig. 4). Low-temperature reorganization reactions are hard to suppose for the formation of the core-mantle textures. They may be a texture that primarily crystallized Pl was resorbed or replaced by later crystallized Af under magmatic conditions. This process may be comparable to that of the formation of two-feldspar textures as high-temperatures. (Harlov et al., 1998).

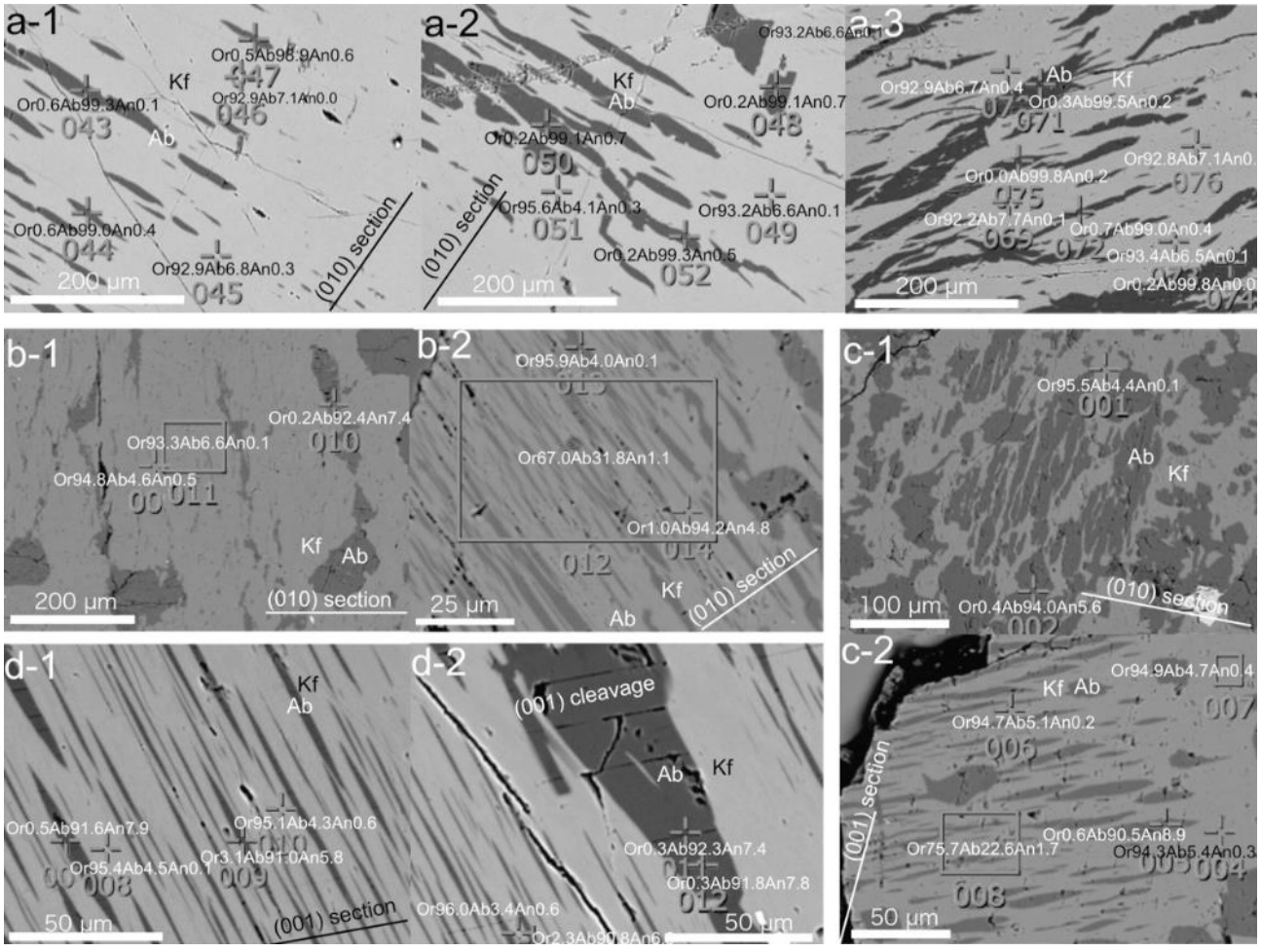

Figure 9. Compositions of constituent two feldspars in individual local areas of the DAIC microperthites, which were obtained by FE-SEM EDS. Crosses show locations of point analyses. Squares show analytical areas of local bulk compositions by area scan analyses. (a) = (001), (b) = (001), (c) = (001), (d) = (010).

We consider at present that the SC-Kf formation may have been formed at the last stage of Af crystallization. The magmatic textures may have become the basis of later reactions reorganizing them and forming the present DAIC feldspar textures. The primarily heterogeneous or chaotic distributions of Ab feldspars and non-microperthitic LMKfs are considered to have been reorganized and modified by multi-stage reactions of later exsolution and pervasive low-temperature reorganization (replacement).

10.3. Exsolutions

Cryptoperthites and fine microperthites observed in the DAIC microperthites are shown in Figs. 7 and 9. The FE-SEM resolves lamellae around 50 nm in width (Nakano et al., 2016). In the samples 9539 and 9535, very fine lamellae somewhat below 50 nm and fine lamellae around 200 nm are scattered between coarser lamellae around 2 μm (and much coarser patches). In the remained samples, individual finest lamellae are around 1 μm in width. These cryptoperthites (and fine microperthites) are considered to be exsolution

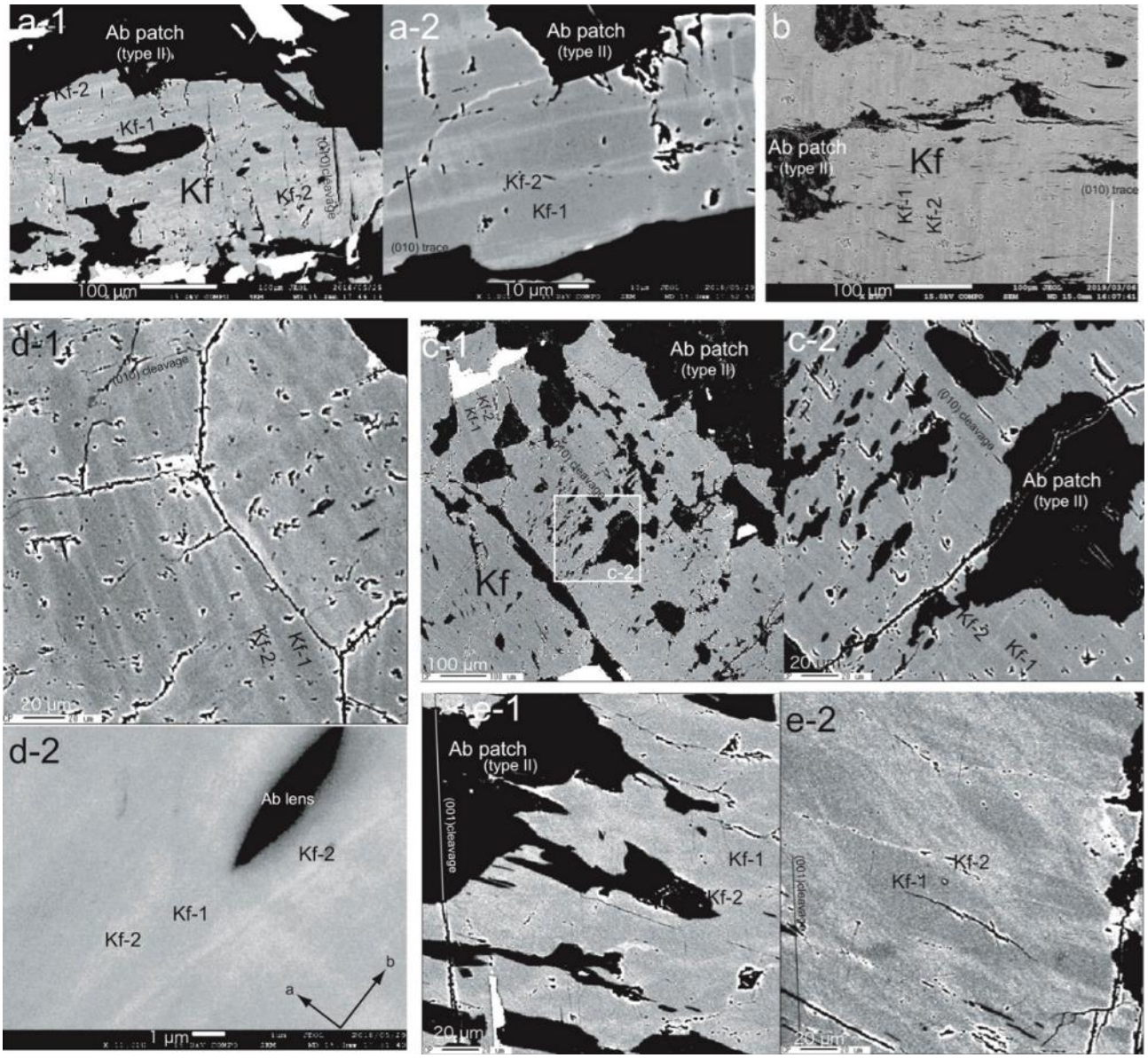

Figure 10. BSE images ((c), (d-1) and (e)) and FE-SEM images ((a), (b) and (d-2)) showing replacement textures of Kf-1 (relatively Or-poorer) by Kf-2 (relatively Or-richer and closer to the end member composition. (a) ample 9547 = roughly (001) showing fine Kf-2 bands elongated along the b-axis direction in Kf-1, (b) sample 129 = (001) showing vertically elongated (roughly along the b-axis direction) Kf-2 bands in Kf-1 between turbid Ab patches (type II), (c) sample 9546 = (001) showing Kf-2 bands elongated along the a-axis direction, (c-2) is an enlarged image of a square part in (c-1), (d) sample 9536=(001) showing Kf-2 bands elongated along the a-axis direction in Kf-1, (d-2) showing crossing Kf-2 bands around an Ab lense of 1 μm in width, (f-1) sample 9535 = (010) showing irregular vein~patch-like Kf-2 in Kf-1 around Ab patches, (f-2) sample 9535 = (010) showing braid-like bundled of fine streak-like Kf-2 in Kf-1.

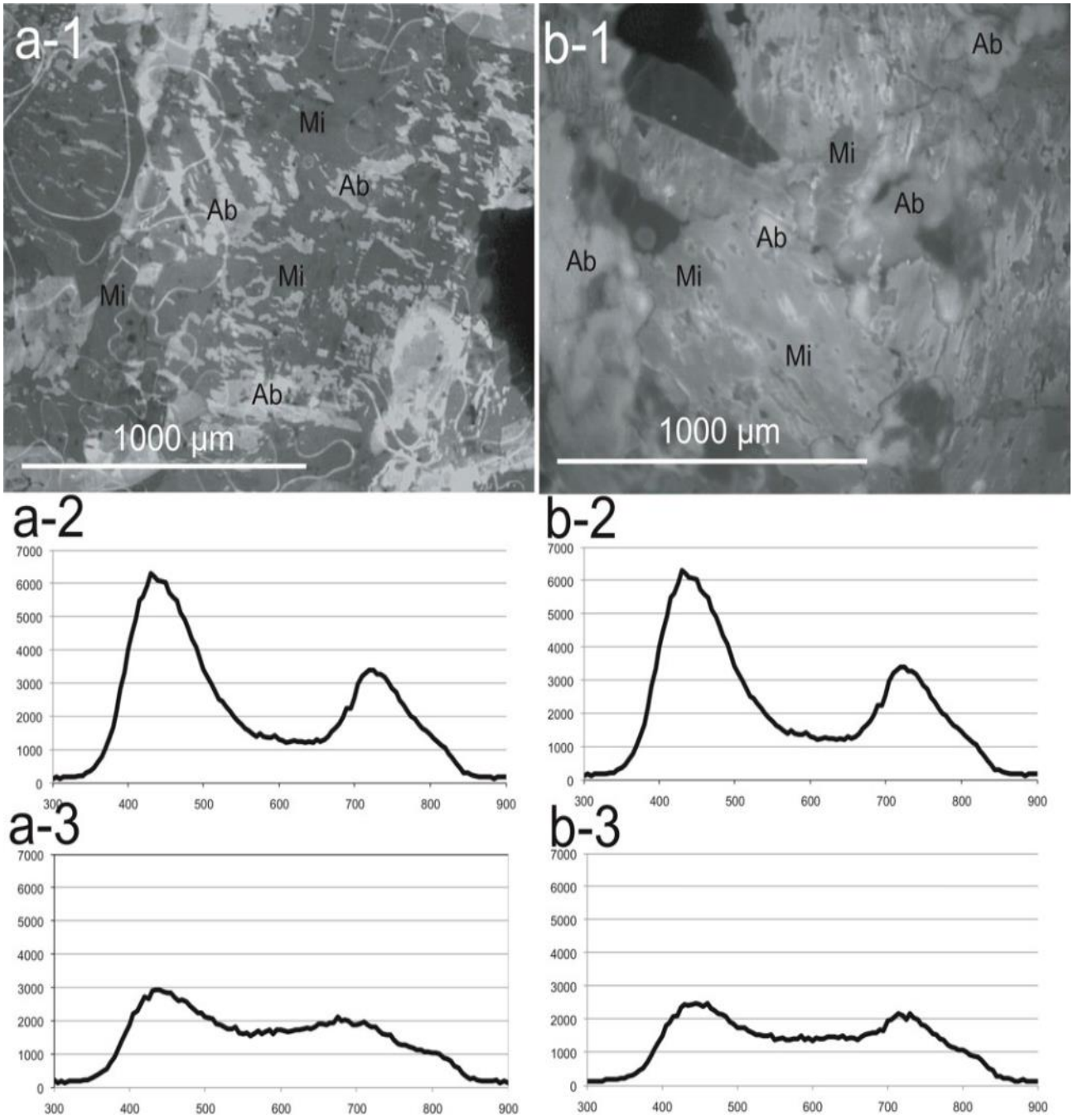

Figure 11. Representative CL images by a luminoscope and spectra obtained by a spectrometer attached to EMPA. (a) sample 129, (b) sample 9535.

products. Coarsening of cryptoperthites may have occurred like the cases of crypto~microperthitic textures almost free of micropores in deformed rocks (Tohver et al., 2005) and granulites (Tajčmanová et al., 2012), in which microperthites have been coarsened from primary cryptoperthites by intracrystalline diffusion. In spite of the textural similarity, however, the DAIC microperthites are very different from them in the compositions. As already stated, the compositions of microperthite constituent feldspars in the DAIC felsic rocks are very close to the end member compositions, which is indicative of later K-feldspathization and albitization after the exsolution and subsequent coarsening processes.

The heterogeneous or chaotic distributions of microperthitic, meso-perthitic and non-microperthitic textures (Figs. 3, 4 and 5) are not interpreted simply as exsolution and coarsening of cryptoperthites, but may be totally interpreted to be due to the multi-stage replacement reorganization from the magmatic crystallization to later K-feldspathization and albitization through exsolution stage.

10.4. Greater compositional and textural reorganizations

10.4.1. Textures

Plutonic microperthites are formed from cryptoperthites by hydrothermal dissolution and reprecipitation reactions with the aid of catalyzers such as water (Guthrie & Veblen, 1991; Hashimoto et al., 2005a, b; Parsons et al., 2013 Nakano et al., 2014a, b). Such so-called hydrothermal microperthites are associated with microscopic turbidity due to the presence of numerous micropores that inevitably form in low temperature dissolution and reprecipitation reactions (Worden et al., 1990; Walker et al., 1995; Putnis, 2002; Putnis & Putnis, 2007). In the DAIC, there is no clear textural evidence (Figs. 3, 4 and 5) that for stress-driven coherently coarsened film microperthites were crosscut or reconstructed by turbid patch microperthites. In contrast, turbidity appears to be very limited especially in and around large Ab core Abs and Ab patches of the type II. Micropores are very scarce in most of LMKf areas and SC-Kfs, and, moreover, in or around most of microperthitic Ab strings~lenses~bands or even in the type I patches (Figs. 4, 5, 6 and 8). This fact is enigmatic from the viewpoint of low-temperature replacement reactions in Afs.

10.4.2. Compositions

The feldspar compositions close to those of the end members are indicative of very low-temperatures. Such paired compositions of Ab and Kf are common to those in the DAIC microperthites, but few in the literature: such few examples are (1) ultra-porous late Ab-rich and Or-rich patch microperthites from the Klokken syenite intrusion (Parsons & Lee, 2009), (2) replacive Ab-rich and Or-rich feldspars in granite microperthites (Lee & Parsons, 1997; Hashimoto et al., 2005a), (3) flame microperthites in deformed rocks (Pryer & Robin, 1995), and (4) meso-microperthites in metamorphosed granites (Day & Brown, 1980), all of which were all attributed to replacement reactions in the feldspars. Curiously, however, the present microperthitic textures are rather different from the examples of (1) and (2) of a low-temperature deuteric origin, but are partly similar to the example (3) of a high-temperature metasomatic origin, and the meso-microperthitic textures in the sample 111 are comparable to the example (4) of a metamorphic origin. This issue is discussed below. In conclusion, anyway, the extensive compositional reorganization is common in the DAIC microperthites. The degree of albitization appears to have been more intense from the sample 9535, toward the sample 111, meaning from the Monzonite-syenite complex toward the Complex of muscovitized syenite, but that of K-feldspathization is not so different through the samples.

10.4.3. Replacement stage

The DAIC microperthites in the examined samples consist of Abs and LMKfs, most of whose compositions are close to the end-member compositions (Table 1, and Figs. 7 and 8). According to any solvus proposed in the Or-Ab binary system (Smith & Brown, 1988; Brown & Parsons, 1989; Deer et al., 2001), the temperatures down to 100°C are estimated from such extreme compositions of the constituent two feldspars. However, local compositional pairs (Fig. 9) do not lie on the same temperature lines on the Or-Ab solvus, which shows that they are not in equilibrium. Although exsolution temperatures vary depending on An contents in Afs (e.g., Parsons & Brown, 1983; Lee & Parsons, 1997), An contents in the DAIC Afs are not so high probably due to the Ca-loss. Even if considering the An effect, the temperatures are roughly estimated to be 200-100°C from the solvus.

However, this low-temperature estimation is intriguing due to the textural similarity to high-temperature textures such as flame perthites, dominant clearness of the feldspars and few of micropores as already mentioned. Higher-temperature hydrothermal replacement experiments by Niedermeier et al., (2009) and Norberg et al., (2011) produced two-feldspar textures of rather extreme compositions texturally similar to some of the DAIC microperthites, in which pure Ab were replaced by pure orthoclase at 600°C with the formation of patch, lens and string Ab remnants almost free of micropores. And, Norberg et al., (2011) produced saw-tooth boundaries and blade shapes of two feldspars by hydrothermal replacement experiments at 500°C, in which orthoclase nearly of the end member composition was replaced by two types of almost pure Ab with micropores and without micropores. In the above two studies, two-feldspar boundaries are sharp and clear. The DAIC microperthites are similar to these synthetic textures. From this similarity, the DAIC microperthits may be considered to have been produced by kinetically controlled interactions between feldspars and fluids at higher temperatures than apparently estimated by the solvus compositions.

10.4.4. Twin genesis

LMKFs showing tartan twin are commonly developed through the samples except for the sample 111. Although tartan twins in microcline are

generally produced by strain release caused by the phase transformation or Si-Al ordering during temperature falling (Smith, 1974; Smith & Brown, 1988; Deer at al., 2001), Waldron et al. (1993) reported low temperature tartan microcline formed at temperatures of 350-400°C by dissolution and reprecipitation locally in granulite microperthites. On the other hand, it has been reported that such twin may be formed during the direct growth as a triclinic phase at low temperatures (Smith & McLaren, 1983; McDowell, 1986). In the case of transformation from higher-temperature structural states in plutonic feldspars, tartan twins develop through several steps from the boundaries to Ab-rich feldspars in the host Or-rich feldspars. In the DAIC microperthites, any textural relation between twin patterns and microperthitic consituent Abs are not observed. There is no clear evidence that they are growth twins too, but the twin genesis during the K-feldspathization is possibly supposed.

In the DAIC microperthitic LMKf, fine bands or veins of the Or-richest compositions were sometimes observed by FE-SEM observations (Fig. 10), which are different from K-feldspathization patterns in microperthites of granitic rocks (Lee & Parsons, 1997; Hashimoto et al., 2005b). Considering their elongation orientations along the a- or b-axis (Fig. 10), these may correspond to secondary compositional fluctuations after primary twin formation as proposed by Sánchez-Muñoz et al. (2006). The present strong blue emissions of LMKf may be comparable to those of a tartan-twinned microcline from a pegmatite (Sánchez-Muñoz et al., 2006), which are caused by variable elastic strain. In contrast, non-luminescent areas indicating low-temperature fluid-feldspar reactions (Finch & Klein, 1999; Sánchez-Munoz et al., 2006; Lee et al., 2007; Kayama et al., 2010) were not detected by CL-imaging in the LMKf. The above compositional and CL data seem to be consistent with the secondary reorganization reactions in the LMKf and SC-Kf tartan twins during the temperature down as demonstrated by Sánchez-Muñoz et al., (2006). This process may have occurred during the progressive K-feldspathization and albitization. In contrast, polysynthetic Ab twin patterns are rarely present in the microperthite Abs, and they are vaguely observed. This suggests that originally generated Ab twin in primary Pl was progressively modified or erased by later reorganization or albitization.

10.5. Nomenclature of syenite

Concerning the reorganization of the DAIC felsic rocks, there is an important issue about the rock nomenclature. The six samples except for the sample 111 are primarily subsolvus rocks. The syenite sample 111 consisting only of meso-microperthitic grains may be apparently recognized to be a hypersolvus rock as well as the previously reported high-temperature hypersolvus syenites (Fuhrman et al., 1988; Oba et al., 1997) and granulites (Yund & Ackermand, 1979; Hayob et al., 1989; Voll et al., 1994; Raase, 1998; Yoshimura et al., 2000; Hokada, 2001; Hartmann et al., 2008). However, the sample 111 mesoperthites consisting of the feldspars showing rather extreme compositions are entirely different from their compositional pairs. The compositions are indicative of later great reorganization by replacement as already stated. Therefore, the sample 111 is a subsolvus syenite, if according to the original definition by Tuttle & Bowen (1958) who classified such syenite to the type IIC granites undergone later recrystallization. These extreme feldspar compositions of this syenite are comparable to those of hydrothermally formed episyenites (e.g., Petersen & Eliasson, 1997).

11. CONCLUSIONS

Irregular zoning patterns of Pls and core-mantle textures with saw-tooth boundaries and “torn textures” in the DAIC felsic rocks are considered product of primarily magmatic crystallization in open system. Cryptoperthite~fine-microperthites are considered to be of exsolution and coarsening origin. The large heterogeneities of microperthites are considered to be accumulated products of magmatic crystallization with resorption, exsolution and coarsening, and later reorganization of albitization and K-feldspathization. As a whole, microperthitic textures are not so similar to well-known low-temperature hydrothermal replacement patch microperthites with turbidity in ordinary granites and syenites, and more similar to microperthitic textures in several types of deformed rocks formed at higher temperatures. The compositional variations of the discrete Pl and constituent two feldspars of the microperthites are in the short range, and most of them are close to the end member compositions Ab and Or, which are indicative of low-temperature K-feldspathization and albitization. However, the reorganization of K-feldspathization and albitization may have occurred at higher temperatures than suggested by the compositions. It is concluded through the DAIC felsic rocks that the feldspar textures and compositions underwent low-temperature greater replacement reactions at the end of the multi-stage reorganizations.

Acknowledgements

We sincerely thank both the Geological Institute of Romania and Faculty of Education, Shiga University for the cooperation to this study. We are also grateful to Yasue Shingu (graduate of Shiga University), Yasufumi Satoguchi of Lake Biwa Museum, Hirotsugu Nishido of Okayama University of Science and Masahiro Kayama of University of Tokyo for their wholehearted help to the study.

REFERENCES

Alling, H.L., 1938. *Plutonic perthites.* The Journal of Geology, 46, 142-165.

Anastasiu, N. & Constantinescu, E., 1982. *Tectonostructural position of the foidic rocks in the Romanian Carpathians.* Studii și Cercetări de Geologie, Geofizică, Geografie, Seria Geologie, Bucuresti 26-33-45.

Batki, A., Pál-Molnár, E., Dobosi, G. & Skelton, A., 2014. *Petrogenetic significance of ocellar camptonite dykes in the Ditrău Alkaline Massif, Romania.* Lithos, 200-201, 181-196.

Batki, A.,Pál-Molnár E., Jankovics É., Kerr A., Kiss B., Markl G., Heincz A. & Harangi, S., 2018. *Insights into the evolution of an alkaline magmatic system: An in situ trace element study of clinopyroxenes from the Ditrău Alkaline Massif, Romania.* Lithos 300-301, 51-71.

Barth, T.F.W., 1969. *Feldspars.* John Wiley & Sons Inc. 261p.

Bindea, G., 1993. *Coexisting albite and oligoclase in some rocks of the Ditrău alkaline massif.* Romanian Journal of Mineralogy, 76, Supplement 1, 9-10.

Bindea, G., 2010. *Aspects and significations of plagioclase disequilibria in the rocks of the Ditrău Alkaline Intrusive Complex Romania.* 2010 Carpathian-Balcan Geological Association Congress, Thessaloniki. Geologica Balcanica, 39, 46-47.

Bonin, B., Tatu M., Bebien J., Bindea G., Demaiffe D., Duchesne J-C., Liegeois J-P., Mărunţiu M., Massol H. & Platevoet B., 2002. *Post-collisional/postorogenic vs. anorogenic alkaline magmatism: the Romanian record.* In "Pan-African Realm Geology" Symposium, Rabat Maroco, 18-24.

Brown, W.L. & Parsons, I., 1989. *Alkali feldspars: ordering rates, phase transformation and behaviour diagrams for igneous rocks. Mineralogical Magazine, 5*3, 25-42.

Day, H.W. & Brown, V.M., 1980. *Evolution of perthitic compositions and microstructure during progressive metamorphism of hypersolvus granite, Rhode Island, USA.* Contribution to Mineralogy and Petrology, 72, 353-365.

Dallmeyer, R.D., Kräutner, H.-G. & Neubauer, F., 1997. *Middle-late Triassic 40Ar/39Ar hornblende ages for early intrusions within the Ditrău alkaline Massif, Romania: implications for Alpine rifting in the Carpathian orogen.* Geologica Carpathica, Bratislava 48m 347-352.

Codarcea, A., Codarcea-Dessila, M. & Ianovici, V., 1957. *Structure geologique du massif des roches alcalines de Ditrău.* Revue de Geologie et Geographie, Academia Română II, 3-4, 385-515.

Deer, W.A., Howie, R.A. & Zussman, J., 2001. *Feldspar minerals 2nd ed.*. Rock-forming minerals Vol. 4A, The Geological Society of London, 972 p.

Fall, A., Bodnar, R.J., Szabo, C. & Pál-Molnár, E., 2007. *Fluid evolution in the nepheline syenites of the Ditrău alkaline massif, Transylvania, Romania.* Lithos, 95, 331-345.

Finch, A. & Klein, J., 1999. *The causes and petrological significance of cathodoluminescence emissions from alkali feldspars.* Contribution to Mineralogy and Petrology, 135, 234-243.

Fuhrman M.L. & **Lindsley D. H**., 1988. *Ternary-feldspar modeling and thermometry*. American Mineralogy 73, 201–215.

Goldich, S.S. & Kinser, J.H., 1938. *Perthite from Torry Hill, Ontario.* American Mineralogist, 24, 407-427.

Guthrie, G.D., Jr. & Veblen, D.R., 1991. *Turbid alkali feldspars from the Isle of Skye, northwest Scotland.* Contribution to Mineralogy and Petrology, 108, 298-304.

Harlov, D.E., Hansen, E.C. & Bigler, C., 1998. *Petrologic evidence for K-feldspar metasomatism in granulite facies rocks.* Chemical Geology, 151, 373-386.

Hartmann, K., Wirth, R. & Markl, G., 2008. *P-T-C controlled element transport through granulite-facies ternary feldspar from Lofoten, Norway.* Contribution to Mineralogy and Petrology, 156, 359-395.

Hashimoto, K., Akai, J. & Nakano, S., 2005a. *Microtextures of alkali feldspar in the Tanakami granite, southwest Japan and their formation processes.* Japanese Magazine of Mineralogical and Petrological Sciences, 34, 1-14. in Japanese with English abstract

Hashimoto, K., Akai, J. & Nakano, S., 2005b. *Microtextures of alkali feldspars in the Kan-nonji granodiorite.* Shiga, Japan. Earth Sciences Chikyu Kagaku, 59, 117-124. in Japanese with English abstract

Hayob, J.L., Essene, E.J., Ruiz, J., Ortega-Gutierrez, F. & Aranda-Gomez, J.J., 1989. *Young high-temperature granulite from the base of the crust in central Mexico*. Nature, 342, 265-268.

Herbich, F., 1872. *Die geologischen Verhältnisse des nordöstlichen Siebenbürgens.* Mitteilungen aus dem Jahrbuche der Kaiserlich ungarischen Geologischen. Anstalt, 2. 293-350, Budapest

Hokada, T., 2001. *Feldspar thermometry in ultrahigh-temperature metamorphic rocks: Evidence of crustal metamorphism attaining ~1100°C in the Archean Napier Complex, East Antarctica.* American Mineralogist, 86, 932-938.

Kayama, M., Nakano, S. & Nishido, H., 2010. *Characteristics of emission centers in alkali feldspar: A new approach by using cathodoluminescence spectral deconvolution.* American Mineralogist, 95, 1783-1795.

Kräutner, H-G. & Bindea, G., 1998. *Timing of the Ditrău alkaline intrusive complex Eastern Carpathians Romania.* Slovak Geological Magazine, 4, 213-221.

Leake, B.E., Wooley, A.R., Arps, C.E.S., Birch,W.D., Gilbert, M.C., Grice, J.D., Hawthorne, F.C., Kato, A., Kirsch, H.J., Krivovichev, V.G., Linthouth, Laird, J., Mandarino, J.A., Maresch, W.V., Nickel, E.H., Rock, N.M.S., Schumacher, J.C., Smith, D.C., Stephenson, N.C.N.,Ungaretti L., Whittaker, E.J.W. & Youzhi G., 1997. *Nomenclature of Amphiboles. Report of the Subcommitte on Amphiboles of the international Mineralogical Association Commission on New Minerals and Mineral Names.* Mineralogical Magazine. April 1997, 61, pp. 295-321.

Lee, M.A. & Parsons, I., 1997. *Dislocation formation and albitization in alkali feldspar from the Shap granite.* American Mineralogist, 82, 557-570.

Lee, M.A., Parsons, I., Edwards, P.R. & Martin, R.W., 2007. *Identification of cathodoluminescence activators in zoned alkali feldspars by hyperspectral imaging and electron-probe microanalysis.* American Mineralogy, 92, 243-253.

McDowell S.D., 1986. *Compositions and structural state of coexisting feldspars, Salton Sea geothermal field*. Mineralogical Magazine, 50, 75-84.

Morogan, V., Upton, B.G.J. & Fitton, J.G., 2000. *The petrology of the Ditrău alkaline complex, Eastern Carpathians.* Mineralogy and Petrology, 69, 227-265.

Nakano, S., 1992. *Internal textures of anti-rapakivi mantled feldspars from Oki-Dogo island.* Mineralogy and Petrology, 46, 123-135.

Nakano, S. & Suwa, K., 1995. *Mantled feldspars in alkali rhyolite from Oki-Dogo island.* Mineralogy and Petrology, 54, 277-289.

Nakano, S., Akai, J. & Shimobayashi, N., 2005. Contrasting Fe-Ca distributions and related microtexrures in syenite alkali feldspar from the Patagonian Andes, Chile. Mineralogical Magazine, 69, 521-535.

Nakano, S., Sawaki, T. & Sasaki, M., 2014a. *Microtexture and compositional variation of alkali feldspars from the Kakkonda granitic pluton, northeast Japan: Implications to the formation processes of granitic texture.* Journal of Mineralogical and Petrological Sciences, 69, 523-537.

Nakano, S., Kutsukake, T. & the Collaborative Research Group for the Granites around Lake Biwa, 2014b. *Hydrothermal reconstruction of the granitoids: As inferred from the mineralogy of the two contrasting Cretaceous granitoid plutons, west to Lake Biwa, Japan.* Journal of Mineralogical and Petrological Science, 43, 184-199. in Japanese with English abstract

Nakano, S., Kojima, S., Makino, K., Kayama, M., Nishido, H. & Akai, J., 2016. *Cryptoperthitic and replacive intergrowths with iridescence in monzonitic rocks from Cerro Colorado, northern Chile.* European Journal of Mineralogy, 28, 355-374.

Nakano, S., Makino, K., Yoshida, I., Maniwa, K.,. Sawada, K Sakashita, F. & Kohno, T., 2019. *Combined influence s of iron-oxides and micropores on reddish coloration of alkali feldspars in granitic rocks.* Journal of Geological Society of Japan, 125-10, 759-773

Niedermeier, D.R.D., Putnis, A., Geisler, T., Golla-Schindler, U. & Putnis, C.V., 2009. *The mechanism of cation and oxygen isotope exchange in alkali feldspars under hydrothermal conditions.* Contribution to Mineralogy and Petrology, 157, 65-76.

Norberg, N., Neusser, G., Wirth, R. & Harlov, D., 2011. *Microtextural evolution during experimental albitization of K-rich alkali feldspar.* Contribution to Mineralogy and Petrology, 162, 531-546.

Oba, T., Uehara, S. & Shiraishi, K., 1997. *Microtexture of perthites in syenites from the Yamato mountains.* East Antarctica. Proceedings NIPR Symposium Antarctic Geosciences, 10, 120-129.

Pál-Molnár E, Batki A, Almási E, Kiss B, Upton BGJ, Markl G, Odling N. & Harangi Sz., 2015a. *Origin of mafic and ultramafic cumulates from the Ditrău Alkaline Massif, Romania.* Lithos 239, 1-18.

Pál-Molnár, E., Batki, A., Ódri Á., Kiss, B. & Almási, E., 2015b. *Geochemical implications for the magma origine of granitic rocks from the Ditrău Alkaline Massif Eastern Carpathians, Romania.* Geologia Croatica, 68 / 1, 51-66.

Pană, D.I., Balintoni, I. & Heaman, L., 2000. *Precise U-Pb zircon dating of the sienite phase from the Ditrău alkaline igneous complex.* Studia Universitatis Babes-Bolyai, Geologia, XLV, no. 1, p. 79-89.

Parsons, I. & Lee, M.R., 2009. *Mutual replacement reactions in alkali feldspars I: microtextures and mechanism.* Contribution to Mineralogy and Petrology, 157, 641-661.

Parsons, I., Fitz Gerald, J.D., Heizler, M.T., Ivanic, T. & Lee, M.R., 2013. *Eight-phase alkali feldspars: low-temperature cryptoperthite, peristerite and multiple replacement reactions in the Klokken intrusion.* Contribution to Mineralogy and Petrology, 165, 931-960.

Petersen, J. & Eliasson, T., 1997. *Mineral evolution and element mobility during episenitization dequartzification and albitization in the postkinematic Bohus granite, southwest Sweden.* Lithos, 42, 123-146.

Pryer, L.L. & Robin, P.-Y.F., 1995. *Retrograde metamorphic reactions in deforming granites and the origin of flame perthite.* Journal of Metamorphic Geology, 13.645-658.

Putnis, A. 2002. *Mineral replacement reactions: from macroscopic observations to microscopic mechanism.* Mineralogical Magazine, 66, 689-708.

Putnis, A. & Putnis, C.V., 2007. *The mechanism of reequilibration of solid in the presence of a fluid phase.* Journal of Solid State Chemistry., 95, 10-18.

Raase, P., 1998. *Feldspar thermometry: a valuable tool for deciphering the thermal history of granulite-facies rocks, as illustrated with metapelites from Sri Lanka.*

The Canadian Mineralogist, 36, 67-86.

Ramberg, I.B., 1972. *Braid perthite in nepheline syenite pegmatite, Langesundsfjorden, Oslo Region Norway.* Lithos, 5-4, 281-306.

Robertson, F., 1959. *Perthite formed by reorganization of albite from plagioclase during potash feldspar metasomatism.* American Mineralogist, 44, 603-619.

Sánchez-Muñoz, L., Correcher, V., Terrero, M.J., Cremades, A. & Garicia-Guinea, J., 2006. *Visualization of elastic starins fields by the spatial distribution of the blue luminescence in a twinned microcline crystal.* Physycs and Chemistry of Minerals, 33, 639-650.

Smith, J.V. 1974 *Feldspar minerals,* Vol.2 Chemical and textural properties, Springer-Verlag Berlin Heidelberg New York, 690pp.

Smith, J.V. & Brown, WL. 1988. *Feldspar Minerals 1*. Springer, Berlin Heidelberg New York, 828 p.

Smith, K.L. & McLaren, A.C., 1983. *TEM investigation of a microcline from a nepheline syenite* Physic and Chemistry of Minerals, 10, 69-76.

Streckeisen, A., 1931. *Über das Nephelinsyenitmassiv von Ditroff Rumänien.* Neues Jahrbuch für Mineralogie, B-B 64, Abt A Brauns-Festschr., 615-628.

Streckeisen, A., 1954 *Das Nephelinsyenit-Massiv von Ditroff Siebenbürgen.* Schweizerische Mineralogische und Petrographische Mitteilungen, 32, 249-310.

Streckeisen, A. 1960. *On the structure and origin of the Nepheline-Syenite Massif, Ditro Transsylvania, Romania.* Report 21th IGC part 13, 228-238.

Streckeisen, A. & Hunziker, J.C., 1974, *On the origin and age of the Nepheline Syenite Massif of Ditro Transsylvania, Romania.* Schweizerische Mineralogische Petrographische Mitteilungen, 54, 59-77.

Tajčmanová, L., Abart, R., Wirth, R., Habler, G. & Rhede, D., 2012. *Intracrystalline microstructures in alkali feldspars from fluid-deficient granulites: a mineral chemical and TEM study.* Contribution to Mineralogy and Petrology, 164, 716-729.

Tohver, E., Pluijm, B.A., Scandolara, J.E. & Essene, E.J., 2005. *Late Mesoproterozoic deformation Rondonia, Brasil: Geochronological and structural evidence for collision with southern Laurentia.* The Journal of Geology, 113, 309-323.

Tuttle, O.F. & Bowen, N.L., 1958. *Origin of granite in the light of exerimental studies in the system* $NaAlSi_3O_8$-$KAlSi_3O_8$-SiO_2-H_2O. The Geological Society of America Memoirs, 74, 153 p.

Vernon, R.H., 1999. *Flame perthite in metapelitic gneisses at Cooma, SE Australia.* American Mineralogist, 84, 1760-1765.

Voll, G., Evangelakakis, C. & Kroll, H., 1994. *Revised two-feldspar geothermometry applied to Sri Lanka feldspars.* Precambrian Research, 66, 351-377.

Yoshimura, Y, Motoyoshi, Y., Grew, E.S., Miyamoto, T., Carson, C.J. & Dunkley, D.J., 2000. *Ultrahigh-temperature metamorphic rocks from Howard Hills in the Napier Complex, East Antarctica.* Polar Research, 13, 60-85.

Yund, R.A. & Ackermand, D.A., 1979. *Development of perthite microstructures in the Storm King granite, N.Y.* Contribution to Mineralogy and Petrology, 70, 273-280.

Waldron, K.A., Parsons, I. & Brown, W.L., 1993. *Solution-redeposition and the orthoclase- microcline transformation: evidence from granulites and relevance to 18O exchange.* Mineralogical Magazine, 57, 687-695.

Walker, F.D.L., Lee, M.R. & Parsons, I., 1995. *Micropores and micropermeable texture in alkali feldspars: geochemical and geophysical implications.* Mineralogical Magazine, 59, 505-534.

Wen, S. & Nekvasil, H., 1994. *Solvcalc: an interactive graphic program package for calculating the ternary feldspar solvus and for two-feldspar thermometry.* Computer & Geosciences, 20. 1025-1040.

Worden, R., Walker, F.D.L., Parsons, I. & Brown, W.L., 1990. *Development of microporosity, diffusion channels and deuteric coarsening on perthitic alkali feldspars.* Contribution to Mineralogy and Petrology, 104, 507-514.

Received at: 10. 08. 2020
Revised at: 21. 08. 2020
Accepted for publication at: 26. 08. 2020
Published online at: 28. 08. 2020